Architecture of transpressional thrust faulting in the San Bernardino Mountains, southern California, from deformation of a deeply weathered surface

Sieh, Kerry; Spotila, James A.

2000

Spotila, J. A., & Sieh, K. (2000). Architecture of transpressional thrust faulting in the San Bernardino Mountains, southern California, from deformation of a deeply weathered surface. Tectonics, 19(4), 589–615.

https://hdl.handle.net/10356/95548

https://doi.org/10.1029/1999TC001150

TECTONICS, VOL. 19, NO. 4, PAGES 589-615 AUGUST 2000

Architecture of transpressional thrust faulting in the San Bernardino Mountains, southern California, from deformation of a deeply weathered surface

James A. Spotila

Department of Geological Sciences, Virginia Polytechnic Institute and State University, Blacksburg

Kerry Sieh

Division of Geological and Planetary Sciences, California Institute of Technology, Pasadena

Abstract. To investigate the architecture of transpressional deformation and its long-term relationship to plate motion in southern California, we have studied the deformation pattern and structural geometry of orogeny within the San Andreas fault system. The San Bernardino Mountains have formed recently at the hub of several active structures that intersect the San Andreas fault east of Los Angeles. This mountain range consists of a group of crystalline blocks that have risen in association with transpressive plate motion along both high- and low-angle faults of a complex structural array. We have used a deeply weathered erosion surface as a structural datum to constrain the pattern of vertical deformation across fault blocks in and adjacent to this mountain range. By subtracting the hanging wall and footwall positions of this preuplift horizon we have determined vertical displacement along two major thrust faults. We conclude that one fault, the North Frontal thrust, has played a more significant role in raising the large fault blocks and can explain the uplift of all but a few crustal slivers. On the basis of the pattern of displacement associated with this thrust fault we have also inferred fault zone geometry beneath the range. Rather than simply steepening into a high-angle fault zone or flattening into a decollement, the thrust fault may have a complex, curviplanar geometry. The pattern of rock uplift also enables us to calculate the total motion accommodated by this orogeny. We estimate that >6 km of convergence.(5% of the total plate motion in the last 2 Myr) has occurred. This horizontal shortening is associated spatially with the 15-km-wide restraining bend in the San Andreas fault zone near San Gorgonio Pass. The entire range may thus have risen because of a small geometric complexity in the San Andreas fault rather than the obliquity of far-field plate motion.

1. Introduction

By definition, continental transform plate boundaries are dominated by horizontal plate motions. However, along transpressive or transtensional margins, where significant obliquity between plate motion vectors and plate boundaries exists, strike-slip displacement alone cannot adequately accommodate relative movements of the lithosphere [*Dewey et al.*, 1998]. Instead, far-field horizontal plate motions are manifest as complex deformation along the plate boundary, which can involve significant vertical strain [*Teyssier et al.*, 1995]. The accommodation of horizontal plate motion by convergent or divergent structures is not a simple process, and its characteristics are not predicted by simple tectonic theory. As a result, there are many models of transpressive deformation that are debated in terms of geometry [e.g., *Sylvester*, 1988; *Lemiski and Brown*, 1988] and mechanics [e.g., *Wilcox et al.*, 1973; *Mount and Suppe*, 1987] of structures.

In southern California the obliquity between plate motion direction and the San Andreas fault system, the primary transform, is 27° [*DeMets*, 1995] (i.e., the "Big Bend"; Figure 1). The resulting oblique convergence is accommodated in the far field by a wide fold and thrust belt (the western Transverse Ranges [*Namson and Davis*, 1988]). In the near field the San Andreas fault exhibits nearly pure strike-slip displacement, although localized rock uplift has occurred within the fault zone itself (e.g., Yucaipa Ridge [*Spotila et al.*, 1998]) and across narrow belts associated with local geometric perturbations of the fault zone (e.g., the restraining bend at San Gorgonio Pass [*Allen*, 1957; *Jones et al.*, 1986]). Oblique plate motion is thus accommodated by two architectures of deformation: wide, internally deforming thrust sheets (i.e., decollements) and narrow, high-angle zones (i.e., flower structures). These general cases mimic the two broad architectures that have been observed elsewhere in transpressive environments [*Sylvester*, 1988; *Lemiski and Brown*, 1988; *Lettis and Hanson*, 1991; *Vauchez and Nicolas*, 1991; *Beaudoin*, 1994]. However, the relationship between these deformation styles is not clear. First, it is not obvious why two styles exist. Does far-field deformation represent distributed slip partitioning due to oblique convergence, while near-field deformation results from local geometric complexities along the strike-slip fault itself? Second, it is not clear how low-angle and high-angle deformation zones interact at intermediate distances from strike-slip fault zones. Do thrust faults merge with the strike-slip zone itself, or are they completely decoupled in the subsurface?

Paper number 1999TC001150.
0278-7407/00/1999TC001150$12.00

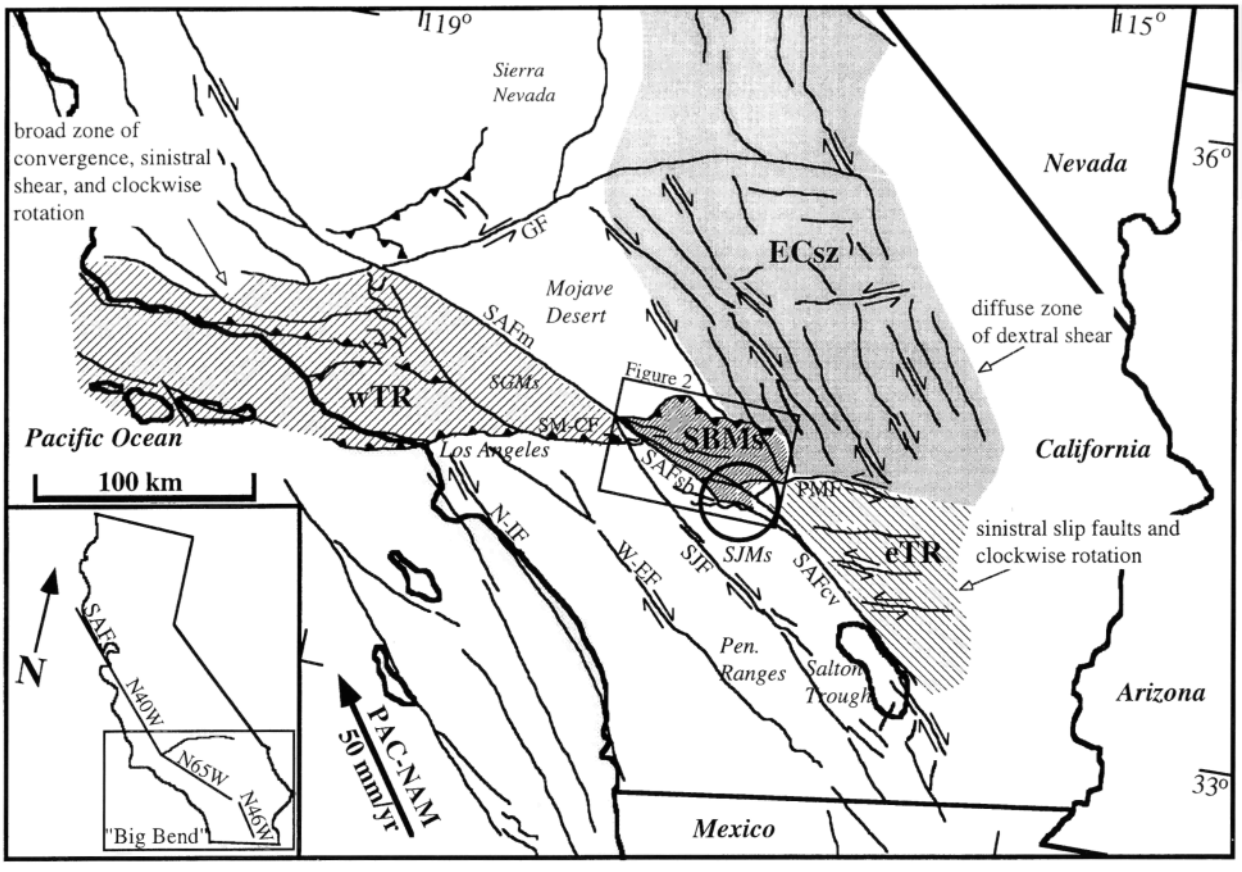

Figure 1. Active tectonic context of the San Bernardino Mountains (SBMs). The "Big Bend" of the San Andreas fault occurs south of the Garlock fault (GF) and north of the small restraining bend at San Gorgonio Pass (circle). Relative plate motion vector is from *DeMets* [1995]. ECsz, eastern California shear zone (gray); eTR, eastern Transverse Ranges (ruled); N-IF, Newport-Inglewood fault; Pen. Ranges, Peninsular Ranges; PMF, Pinto Mountain fault; SAF, San Andreas fault (m, Mojave; sb, San Bernardino; cv, Coachella Valley segments); SGMs, San Gabriel Mountains; SJF, San Jacinto fault; SJMs, San Jacinto Mountains; SM-CF, Sierra Madre-Cucamonga fault; W-EF, Whittier-Elsinore fault; wTR, western Transverse Ranges.

To better understand how horizontal plate motion is manifest as crustal deformation along transpressive strike-slip fault systems, the architecture and kinematic history of structural arrays at intermediate distances to strike-slip fault zones must be quantified. The San Bernardino Mountains (SBMs) extend from near-field to intermediate distance from the San Andreas fault zone (Figure 1) and have been elevated over the past few million years in association with transpressive deformation [*Dibblee,* 1975; *Meisling and Weldon,* 1989; *Spotila et al.,* 1998]. This young mountain system thus represents an ideal opportunity to study long-term transpressive orogenesis associated with the San Andreas fault system. The bulk of the range consist of the broad Big Bear plateau, which has been raised along two east-west trending thrust faults with opposing dips (North Frontal thrust system (NFTS) and Santa Ana thrust (SAT)) (Figure 2). Critical to understanding the structural kinematics of the SBMs is knowing whether the subsurface geometry of these thrusts mimics the high-angle deformation observed within the San Andreas fault zone or the low-angle deformation that occurs at greater distance from its trace. Although both have been proposed as models for the SBMs [*Sadler,* 1982; *Li et al.,* 1992], the subsurface structural geometry and displacements of the faults have not been well constrained. Previous efforts have been stymied because the SBMs consist mainly of crystalline bedrock that cannot be palinspastically restored in balanced cross sections.

We have used a geomorphic feature as a structural datum to quantify the pattern of rock uplift in the SBMs and thereby place constraints on the displacement and geometry of the major structures. Atop the SBMs and across the surrounding lowlands is a low-relief, deeply weathered, granitic erosion surface (Figure 3). Geologic and geomorphic relationships argue that this surface is relict, in that it formed prior to recent mountain building and was subsequently separated by the major thrust faults of the range [*Oberlander,* 1972; *Meisling,* 1984; *Spotila,* 1999]. We have used the distribution of this easily identified geologic marker to reconstruct the vertical

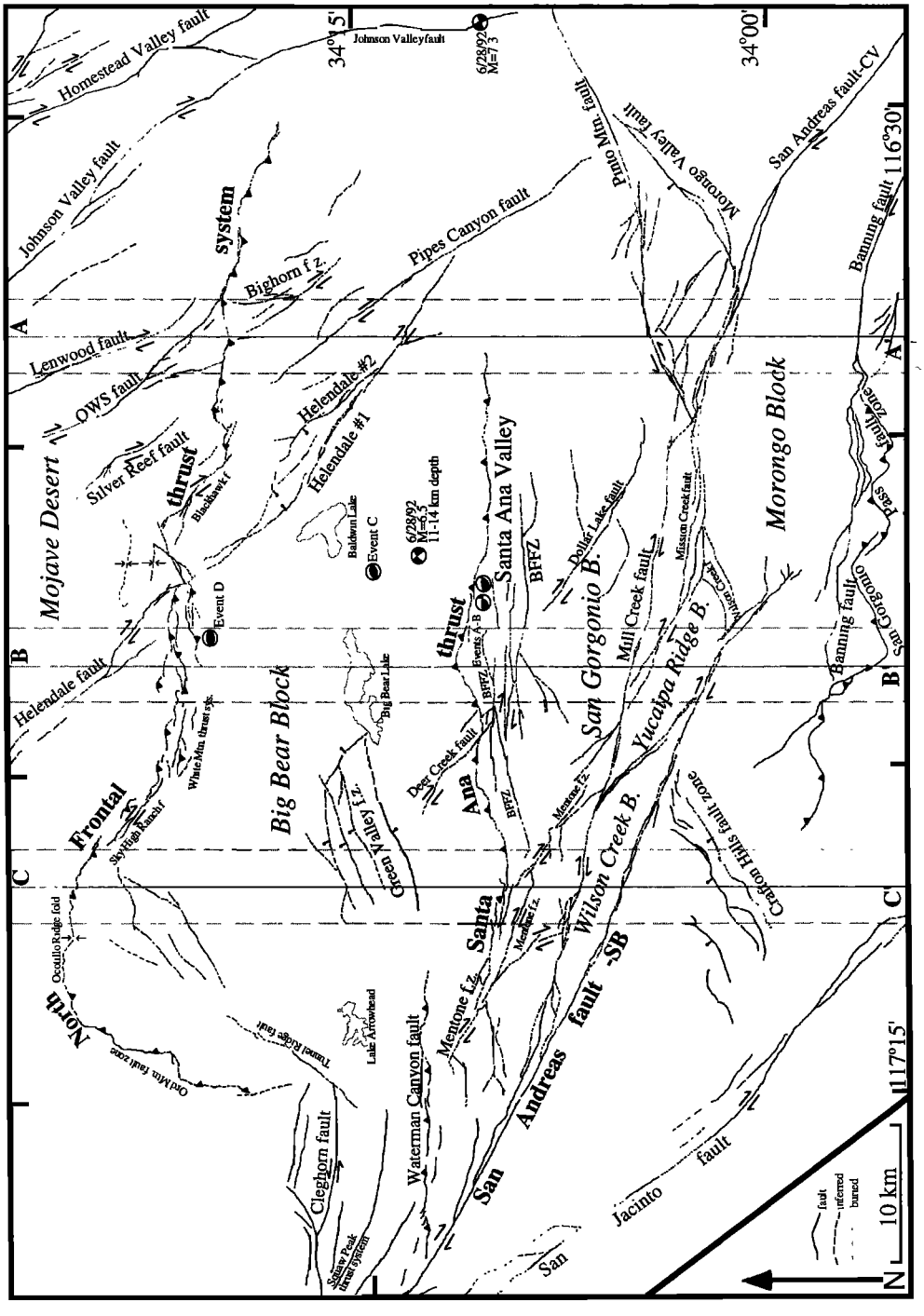

Figure 2. Tectonic map of the SBMs, with all significant active faults and folds and major structural blocks of the range. The North Frontal thrust system (NFTS) and Santa Ana thrust (SAT) are dominant east-west trending thrust faults. The San Andreas fault zone and the northwest trending dextral slip faults within and to the north of the range are also important. Arrows denote strike-slip motion, teeth denote thrust motion, and solid circles denote downthrown sides of normal faults. Distribution of faults is based on airphoto mapping at 1:50,000 scale [*Spotila*, 1999], as well as previous work in the western part of the range [*Meisling and Weldon*, 1989]. Beach balls show location and focal mechanisms at epicenters of important recent earthquakes in the region [E. Hauksson, manuscript in preparation, 1999]. Lines AA', BB', and CC' show cross-section locations (Figure 9). The dashed lines on either side represent the window used to plot seismicity on profiles AA', BB', and CC' (Figure 11). B, block; BFFZ, Barton Flats fault zone; CV, Coachella Valley strand; f.z., fault zone; OWS, Old Woman Springs fault; SB, San Bernardino strand.

displacement field with some certainty. Our results demonstrate that the NFTS has been the dominant structure responsible for uplift of the SBMs and likely undercuts the SAT at depth. On the basis of the pattern of rock uplift we propose a complex subsurface structural geometry that bears similarity to both high-angle and low-angle models of transpressive deformation. The pattern of vertical displacement also suggests a link between horizontal shortening in the SBMs and the restraining bend in San Gorgonio Pass. These results provide important new insight on the architecture of deformation in the SBMs and improve our understanding of transpressive orogenesis. Our constraints on fault geometry and displacement also help characterize regional seismic hazards.

2. Geological Background

The North Frontal thrust system bounds the 80-km-long northern range front, an impressive escarpment with ample geomorphic indicators of recent uplift [*Bull,* 1977; *Miller,* 1987] (Figure 3). It displays pure thrust motion and is considered a fault system because it consists of a complex, kilometer-wide band of discontinuous fault strands and folds [*Meisling and Weldon,* 1989; *Sadler,* 1982]. The fault has juxtaposed crystalline basement over Plio-Pleistocene sediments, including the Old Woman Sandstone [*Woodford and Harriss,* 1928; *Dibblee,* 1975]. Clast provenance, paleocurrents, and facies in this unit record the initiation of the thrusting as post 2-3 Ma [*May and Repenning,* 1982; *Sadler,* 1982]. Late Pleistocene alluvium is also extensively faulted along the northern range front, with scarps locally reaching heights of 60 m [*Meisling,* 1984; *Miller,* 1987]. Although a segment of the NFTS has been seismically active as recently as 1992 (M5.4 [*Feigl et al.,* 1995]), Holocene scarps occur only locally [*Bryant,* 1986]. Thus there is debate as to whether the fault is as active today as it has been throughout the Pleistocene [*Meisling and Weldon,* 1989; *Miller,* 1987]. The northern margin of the plateau is penetrated by northwest trending dextral faults of the eastern California shear zone (Figure 2), which could indicate that thrusting has been replaced by strike-slip deformation. Although the occurrence of these faults in both the upper and lower thrust plates has been used as an argument that the NFTS is largely inactive [*Sadler,* 1982], no clear crosscutting relationship or direct connection between faults north and south of the NFTS have been mapped [*Miller,* 1987]. Thus these two fault systems might both be active [*Spotila,* 1999].

The Santa Ana thrust bounds only a portion of the southern margin of the plateau (Figure 3). Its escarpment is also high and rugged, indicating the important role of the SAT in uplifting the plateau relative to the low Santa Ana Valley to the south (Figure 2). The disappearance of the escarpment eastward into high mountainous topography, however, shows that the SAT could have been responsible for uplifting only a fraction of the SBMs (Figure 3). The fault has juxtaposed basement over the Mio-Pliocene Santa Ana Sandstone [*Sadler,* 1993]. Basalts in this unit indicate a post-6.2 Ma initiation of thrusting along the southern plateau margin [*Woodburne,* 1975]. Much of the SAT is buried by Quaternary deposits, however, and late Pleistocene scarps occur only locally [*Jacobs,* 1982; *Dibblee,* 1964a, 1974; *Spotila,* 1999]. Some young scarps occur near intersections with northwest trending strike-slip faults and may represent local activity [*Jacobs,* 1982]. The SAT's trace has been disarticulated locally by strike-slip structures. The Deer Creek fault, for example, offsets the SAT by ~200 m dextrally. Complexities near the Mentone fault zone may also indicate disruption of the SAT (Figure 2). This relationship suggests that dextral faults postdate the SAT, but the history of activity along the thrust fault is not well known. On the basis of similarities to the Squaw Peak thrust system to the west, *Meisling and Weldon* [1989] suggested that the SAT was active mainly in the Miocene. The Waterman Canyon fault is a strand of the Squaw Peak thrust system and has similar trend, escarpment, and structural position as the SAT (Figure 2). These two thrust faults may indeed be the same structure. A lack of direct constraints on the timing of the SAT and Waterman Canyon fault, however, yields uncertainty as to whether they were active throughout the Pliocene or terminated during the Miocene.

The subsurface geometry of the NFTS and SAT are not well known. Both thrust faults display a range in dip at the surface (10°-60°) but, on average, dip ~30°-35° toward each other [*Miller,* 1987; *Meisling,* 1984; *Woodford and Harriss,* 1928; *Rzonca and Clark,* 1982; *Jacobs,* 1982]. The NFTS and SAT probably meet at some depth below the plateau, but whether they merge or truncate each other is not known. A seismic reflection profile across the NFTS shows that it retains its low dip in the upper kilometer of crust [*Li et al.,* 1992], but little else is well constrained. One hypothesis for the architecture of these faults is that the NFTS is the main structure responsible for uplift of the plateau and becomes a low-angle detachment at depth that undercuts the SAT. This is based on a southward deepening base of microseismicity (~10°S dip [*Corbett,* 1984]), a similarly oriented zone of high seismic reflectivity [*Li et al.,* 1992], and several small, deep earthquakes with shallow nodal planes [*Webb and Kanamori,* 1985]. An alternative hypothesis is that the two thrusts steepen and merge into a mushroom-shaped, high-angle zone of distributed transpression [*Sadler,* 1982]. This idea is based on the symmetry of the opposing thrust faults, which appear as antithetic structures of roughly similar length and displacement. The displacement patterns along the thrust faults have not been defined, however, and thus their relative roles in accommodating contraction are uncertain. The importance of high-angle transpressive zones is evident in the southern SBMs, where crustal slivers have been uplifted within strands of the San Andreas fault zone [*Spotila et al.,* 1998]. The kinematic relationship between these high-angle, oblique slip faults and the thrust faults to the north, however, cannot be understood until geometry of the thrusts are constrained.

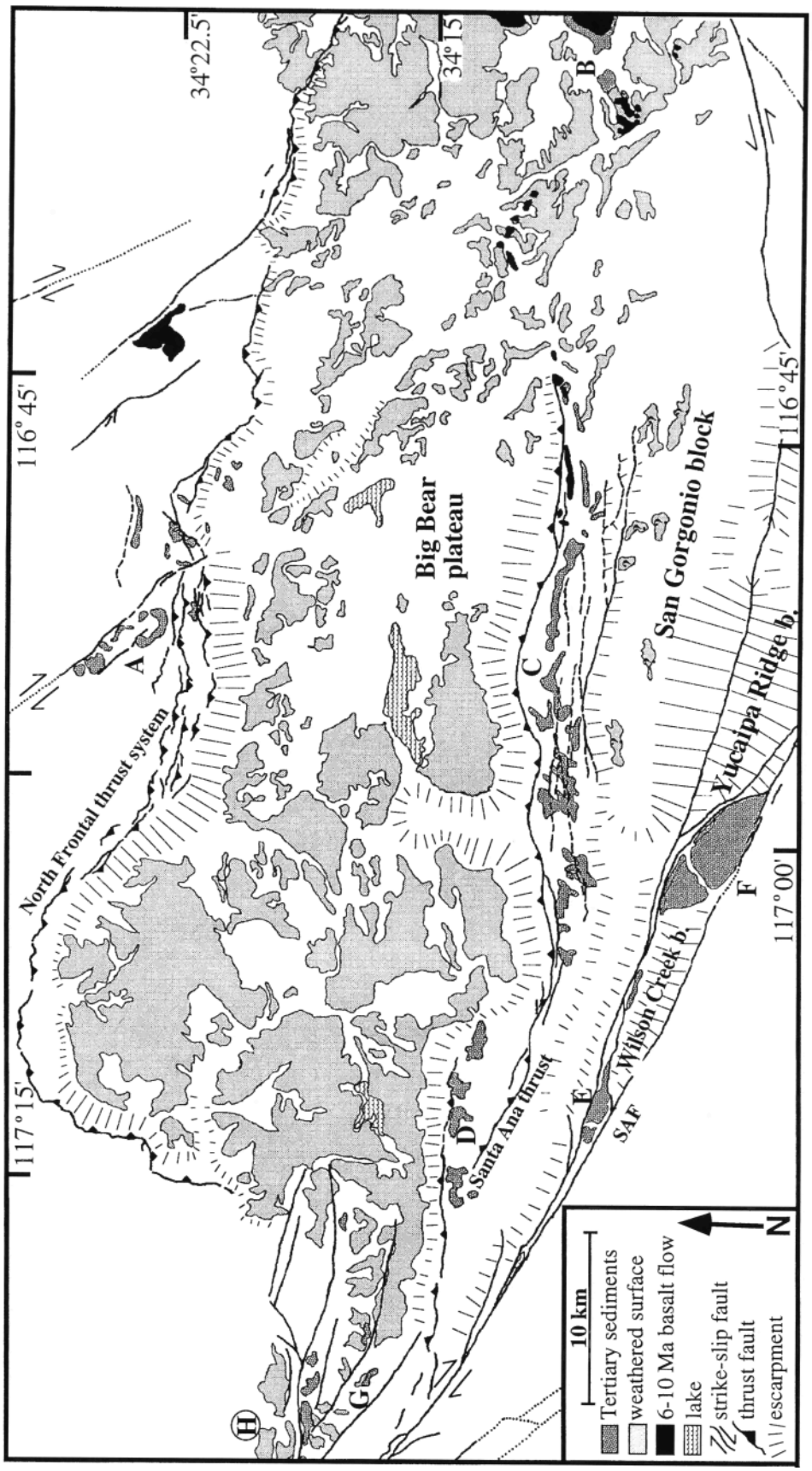

Figure 3. Simplified geomorphic-geologic map of the SBMs showing the distribution of the weathered surface, Tertiary sediments, and basalt within the range. These are critical elements in constraining the recent deformation of the range. The approximate distribution of steep bedrock escarpments appear as a lined pattern, which represents the direction and size of the escarpment. Only major faults of the range that define the major structural blocks are drawn. Letters refer to locations of Tertiary sediments: A, Old Woman Sandstone; B, Santa Ana Sandstone overlying weathered surface; C, central Santa Ana Sandstone; D, eastern Crowder Formation; E, Potato Sandstone; F, Mill Creek formation; G, Crowder Formation overlying weathered surface; H, general location of Cajon, Crowder, and Phelan Peak formations.

Thus the structural pattern within the SBMs is complex. Plate motion has been accommodated by the opposed thrust faults, the high-angle faults in the south, and diffuse dextral faults that penetrate the range on the north, all of which have interacted in the past few million years. Because the subsurface geometry and displacements of these structures are not well known, the functional relationship between plate motion and transpressive orogeny is not well understood. The limiting factor thus far in constraining the architecture of this system is the unconstrained pattern of vertical deformation across the range.

3. Methods

To define the vertical displacement pattern across the SBMs, a widespread, easily identified structural datum is needed. In section 3.1 we describe a deeply weathered erosion surface on granite and how it serves this purpose [*Spotila,* 1999]. We have constructed detailed structure contour diagrams of this weathered horizon throughout both the SBMs (hanging wall of NFTS) and surrounding Mojave Desert (footwall of NFTS). The methods used to define these contours are explained below. Once defined, these contours can be subtracted to determine the vertical displacements on the NFTS and SAT. The displacement field also constrains the subsurface pattern of thrust faulting and the pattern of horizontal plate motion accommodated by uplift. We describe the techniques and results of these structural analyses in the subsequent section.

3.1. Weathered Surface

The Big Bear plateau is characterized by an extensive, low-relief upper surface perched at high altitude (from 1.5 to 2.5 km elevation), which is isolated from surrounding lowlands by steep fault escarpments and canyon walls (Figure 3). While fresh bedrock is exposed along the localized steep slopes, up to 30 m of deeply weathered rock occurs along the gently rolling upland surface [*Spotila,* 1999; *Meisling,* 1984; *Brown,* 1976]. Low-relief patches of deep-weathering also occur atop the San Gorgonio Block, in the structurally low Santa Ana Valley, and in the surrounding Mojave Desert [*Spotila,* 1999; *Jacobs,* 1982; *Oberlander,* 1972] (Figure 3). Rock along these surfaces share the same structural level with respect to thermochronometric isochrons that formed at ~75°C (~3 km depth), suggesting the surfaces were continuous prior to displacement along block-bounding faults [*Spotila et al.,* 1998]. This continuous surface likely developed in a low-energy erosional environment that existed prior to uplift but is now in disequilibrium with its position above base level [*Spotila,* 1999]. The surface's widespread distribution makes it a potential datum to constrain the regional pattern of vertical displacement.

Because the low relief surface exhibits deep weathering, it had to have been accumulating the residuum of rock decay for a long period. This requires that minimal erosion has occurred where the surface is preserved. The surface has experienced zero post-Miocene erosion locally, where 6-10 Ma basalts overlie it on the eastern plateau [*Neville,* 1983] and Mio-Pliocene sediments overlie it on the west (Crowder Formation [*Meisling and Weldon,* 1989]) and in Santa Ana Valley (Santa Ana Sandstone [*Sadler,* 1993]) (Figure 3). Although the lack of overlying units elsewhere prevents the conclusion that the entire surface is relict (i.e., preuplift), other evidence argues that it represents a horizon of minimal synuplift erosion. Where developed on granitic bedrock, the surface consists of corestones and regolith (grus) that represent a typical profile of deep weathering [*Ollier,* 1975]. Argillaceous soils locally cap this saprolite and indicate extreme decay of the original parent rock. Because of the slow rates of chemical weathering on granites in nontropical climates this thickness of weathered debris may have required several million years of isolation from erosion to accumulate [cf. *Spotila,* 1999]. The magnitude of exhumation indicated by thermochronometry is also consistent with minimal erosion atop the Big Bear plateau in the Cenozoic [*Spotila et al.,* 1998]. Wherever preserved, the weathered surface thus represents a horizon that has experienced minimal erosive lowering since uplift initiated. Its shape is therefore primarily a function of paleotopography and subsequent tectonic deformation.

If the weathered surface indicates where surface uplift has equaled rock uplift (i.e., no exhumation), the displacements along faults can be determined by subtracting its position along footwall and hanging wall blocks. If the paleotopography of the surface can be constrained, its present distribution can also be used to constrain the vertical displacement field of blocks and the subsurface geometry of faults. The low-relief surface likely had minor topographic undulations before uplift, owing to an irregular weathering front associated with lateral variations in bedrock weathering rate (i.e., etchplanation [*Twidale,* 1990]). Chemically resistant metamorphic rocks, for example, outcrop an average of ~0.4 km higher than weatherable granitic bedrock atop the plateau [*Spotila,* 1999]. Significant long-wavelength topographic variations, however, were probably absent. The deep etchplanation along the surface would have required a protracted period of weathering during which a nearly horizontal, regional pediment would have developed [*Spotila,* 1999]. The Neogene stratigraphic record also indicates that all but the westernmost SBMs had very low relief prior to the last few million years [cf. *Spotila,* 1999; *Meisling and Weldon,* 1989; *May and Repenning,* 1982; *Sadler,* 1982, 1993; *Allen,* 1957]. Clast provenance in preuplift sediments surrounding the plateau does indicate that minor positive relief existed at what is now the central plateau [*Sadler and Reeder,* 1983]. However, this relief can be explained by the difference in elevation between a granite pediment and localized resistant quartzite that the sediments were derived from. Granitic bedrock may thus have been approximately flat prior to uplift, so that the weathered granitic surface reflects the pattern of vertical displacement.

3.2. Structure Contour Diagram Atop the SBMs

We constructed a structure contour diagram of the weathered surface, on the basis of a detailed map of its

distribution and a screening process that attempted to minimize differences in its original shape (Figure 4). *Spotila* [1999] mapped the entire weathered surface using airphotos and field observations at a scale of 1:62,500 (contour interval is 80 ft (24 m)). From the mapped distribution of the weathered horizon, we selected ~3000 spot elevations following several criteria. Spot elevations were taken from all patches of the surface >0.5 km in width. Each elevation represents an approximate local median in that the lowest pockets and troughs and highest inselbergs and tors were avoided. This minimizes elevation differences associated with variations in the original weathering front geometry. Spot elevations were also selected from the same bedrock type to ensure that elevation differences were not the result of etchplanation. Locations on Figure 4 shown as solid circles are from bedrock of quartz- or biotite-monzonite, whereas solid squares indicate granitic gneiss, granite, or granodiorite bedrock. The resulting spot elevations were contoured by hand at 200 ft (61 m) intervals. Contours were drawn as continuous lines, except where fault escarpments clearly disrupt the weathered surface.

The structure contour diagram exhibits a smoother shape than the present topography. Contours of the weathered surface are higher than present topography where erosion has lowered or removed the weathered horizon, whereas contours are lower than present elevation where resistant, nongranitic bedrock has produced resistant geomorphic forms. Contours increase smoothly in elevation from 3800 ft (1.2 km) on the western rim and 4400 ft (1.3 km) on the eastern rim to 8000 ft (~2.4 km) on the north central rim. The weathered surface also crests near the center of the southern rim of the plateau (~8200 ft (~2.5 km)). Between the northern and southern crests is a slight trough (~7000 ft (~2.1 km)) that gives the weathered horizon atop the central plateau a saddle-like shape. The highest contours occur south of the plateau, however, where traces of the weathered surface rise steeply along the northern flank of the San Gorgonio block (>10,000 ft (>3.1 km)). These southern contours terminate where remnants of weathered granite disappear along the crest of this block.

The structure contours also reveal a complex geometry, which reflects several phenomena. Most noticeable are discontinuities in the surface along major and minor faults (Figure 4). The contours are perpendicular to the northern and southern thrust escarpments of the NFTS and SAT. The southern break in contours separates weathered surface atop the plateau from the weathered granite and Tertiary sediments in the low, tilted Santa Ana Valley (rises from ~3600 (~1.1 km) to ~5600 ft (~1.7 km), from west to east). Many shorter faults also vertically displace the weathered surface, including segments of the inactive Squaw Peak thrust system on the west [*Meisling and Weldon,* 1989] and active strands of the eastern California shear zone on the northeast [*Dokka and Travis,* 1990]. The degree to which the weathered horizon is deformed is not surprising, given that it may be as old as late Miocene and record 10 Myr of faulting within the plate boundary.

Minor variations in structure contours also betray limitations in our ability to reconstruct the fine details of the weathered surface. There are liable to be artifacts from the weathering front's paleotopography and minor erosion in these structure contours. However, we can estimate the resulting uncertainties. Uncertainty due to erosion is small. Locally, erosion of well-developed soils or thick regolith (i.e., grus and saprolite) of the horizon has exposed a hard rind of corestones [*Spotila,* 1999]. The preservation of deep weathering wherever spot elevations have been taken, however, indicates that the magnitude of recent erosion from the surface has been less than the total thickness of the original, characteristic weathered profile (<50 m). The uncertainty associated with the original geometry of the weathering front is somewhat larger. Even within uniform bedrock types, local variations in bedrock weathering rate may have produced small undulations in the weathering front [*Twidale,* 1990]. Our selection process should have avoided most of these undulations. However, hummocky topography is ubiquitous across the weathered surface, and we cannot be sure that small variations (<100 m) in contour elevation are not due to the short-wavelength (~1 km) paleotopography of the weathering front [*Spotila,* 1999].

These two sources of uncertainty should generally work in opposite directions: erosion resulting in contours that should be higher and undulations due to resistant bedrock resulting in contours that should be lower. Conservative confidence limits of the degree to which structure contours locally represent a smooth, near-horizontal, preuplift structural level are thus about ±100 m. We are less certain about the degree to which the surface was level across long wavelengths. As discussed above, however, available data are most consistent with a regional, near-flat pediment prior to uplift. We thus make the assumption that the surface was essentially horizontal prior to analyzing its form.

Additional uncertainty in contours results from sparsity of data. Across parts of the range, weathered granite has been removed by erosion or buried by Quaternary sediments or is absent simply because nongranitic lithologies are present. The contours almost certainly miss details of the weathered horizon's shape across these areas. Across the Big Bear Valley, for example, the contours indicate a gentle saddle shape, although it is uncertain if weathered granite has been removed by erosion from the valley or is presently buried by the alluvium and lacustrine sediment therein [*Brown,* 1976]. Another special case is the Santa Ana Valley, the footwall block of the SAT. Although we determined the elevation of weathered granite in the western valley beneath Tertiary sediments [*Jacobs,* 1982], thick Quaternary fanglomerates obscure its connection to the weathered surface near high Onyx Mountain on the east (Figure 4). Subsurface data in each of these locations would be required to refine the geometry of our structure contours.

3.3. Structure Contour Diagram of the Mojave Desert

North of the NFTS, thick alluvial deposits cover a large portion of the footwall block. Weathered granite occurs on local basement exposures, but sediments obscure much of

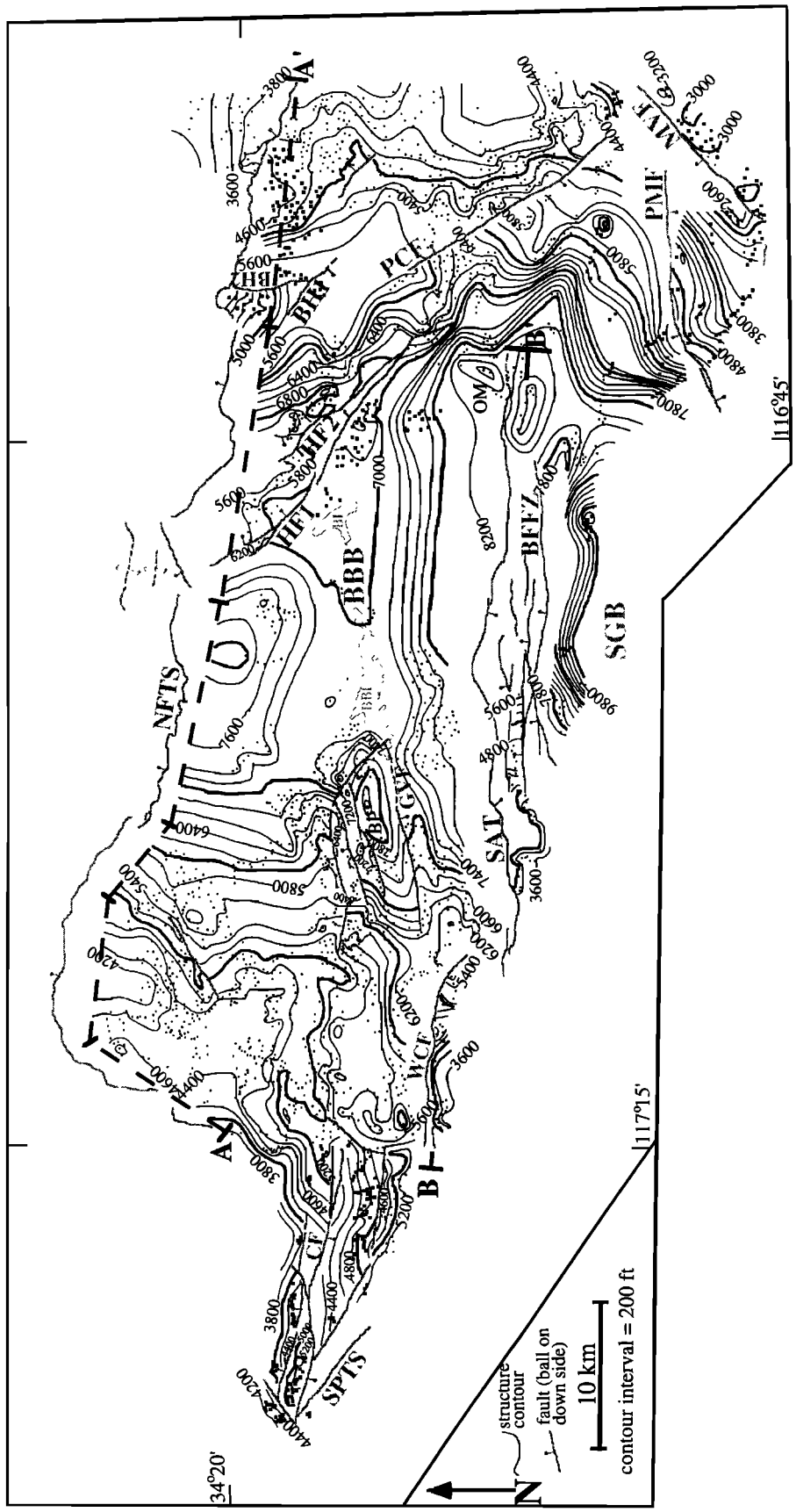

Figure 4. This structure-contour diagram of the weathered surface atop the SBMs is an important datum for restoration of deformation. Darker contours represent 1000 ft (304.8 m) index contours (see Figure 7 for metric version). Only faults that disrupt the elevation of the weathered surface are shown. Solid circles represent elevation data points at which the weathered surface was examined in detail on bedrock of quartz-biotite monzonite. Solid squares are similar but represent observations taken from weathered surface developed on other granitic rock (granitic gneiss, diorites, etc.). BBB, Big Bear block; BBL, Big Bear Lake; BFFZ, Barton Flats fault zone; BH1/2, Bighorn faults; BL, Baldwin Lake; BP, Butler Peak; CF, Cleghorn fault; GVF, Green Valley fault zone; HF1/2, Helendale faults; MVF, Morongo Valley fault; NFTS, North Frontal thrust system; OM, Onyx Mountain; PCF, Pipes Canyon fault; PMF, Pinto Mountain fault; SAT, Santa Ana thrust; SGB, San Gorgonio block; SPTS, Squaw Peak thrust system; WCF, Waterman Canyon fault.

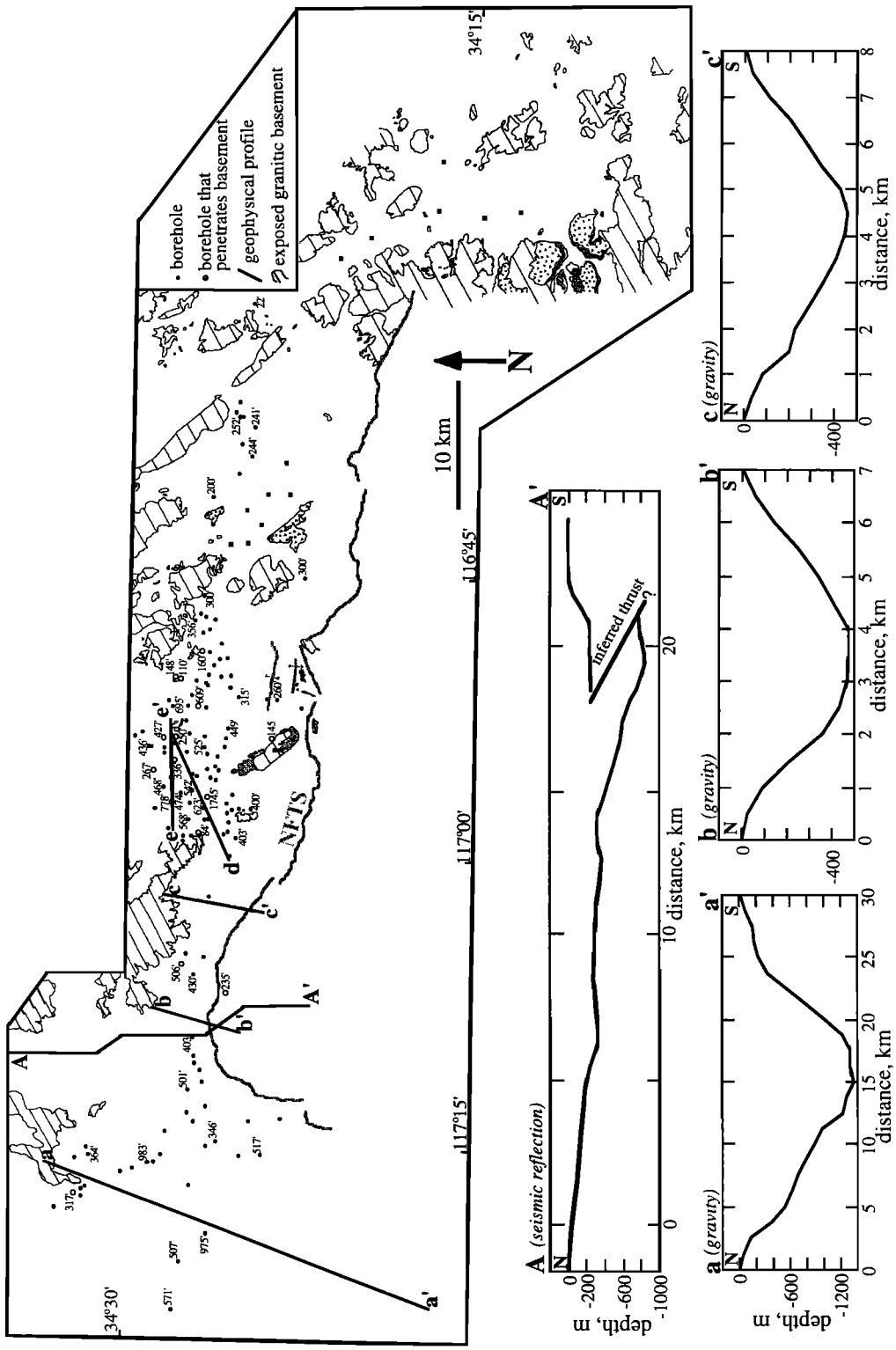

Figure 5. Elevations of granitic basement in the Mojave Desert (footwall block) are necessary input for constructing the structure contours shown in Figure 6. Exposed granitic basement is outlined and filled with a broad-ruled pattern. Lines represent locations of geophysical profiles that constrain the depth to basement. Basement profiles are shown for the interpreted seismic line (AA'; modified from *Li et al* [1992]) and three Bouguer gravity anomaly profiles (aa', bb', and cc'). Basement elevations for dd' and ee' are from *Aksoy et al.* [1986]. Boreholes are shown as circles and are labeled only if used to constrain the minimum depth to basement. Nonlabeled boreholes are very shallow. Open circles indicate boreholes that penetrate basement. All values are given as basement depth below the surface (in meters). Solid squares show locations within alluviated flats on the east, where the depth to basement is known to be <100 m on the basis of a lack of gravity anomalies. Tertiary sediment and basalt are also shown, as in Figure 3.

the weathered surface's distribution (Figure 5). To define structure contours in the footwall block, we thus had to use the elevation of buried basement as a proxy. Because most bedrock in the adjacent Mojave Desert is granitic and capped by a deeply weathered profile [*Oberlander,* 1970], we assume that bedrock beneath alluvium is weathered granite as well. Given the widespread distribution of weathering in the area and the slim chance that basement buried under thick Tertiary and Quaternary deposits experienced greater erosion than the weathered surface atop the exposed Big Bear plateau, we feel that this is a reasonable assumption. We used several data sets to constrain the elevation of buried basement and combined the elevations of exposed weathered granite to construct a structure contour diagram of the weathered surface atop the footwall block.

Existing borehole data provide direct control on the depth to basement north of the range [*Aksoy et al.,* 1986; *Riley,* 1956; *John S. Murk Engineers,* 1985]. Although most wells are very shallow and confined to alluvium, a number penetrate basement or a considerable depth of alluvium and are thus very useful. These deep wells are labeled on Figure 5. A second constraint on the depth to basement is provided by a seismic reflection profile across the western NFTS [*Li et al.,* 1992]. The two-dimensional geometry of the Lucerne Valley basin appears clearly as a reflection from the sediment-basement interface. This contact dips southward and is offset across the NFTS, creating a bedrock wedge in the hanging wall that has overthrust a trapped wedge of alluvium in the footwall . We interpreted basement depths from the two-way travel times on this profile by assuming a 2.5 km/s P-wave velocity for the alluvium (Figure 5).

Another useful constraint for determining the depth to basement is Bouguer gravity data. Basement depth can be calculated from gravity anomalies by assuming a density contrast between unconsolidated sediment and crystalline bedrock. *Aksoy et al.* [1986] determined the depth to bedrock along two profiles in the central Lucerne Valley (dd' and ee' in Figure 5). We calculated three additional depth profiles (aa', bb', and cc') using a two-dimensional modeling program (S. Biehler, personal communication, 1998) on complete Bouguer gravity anomaly data [*Biehler et al.,* 1988] and assuming a 0.4 g/cm^3 density contrast. These profiles are probably accurate to within several hundred meters. We also interpret a lack of gravity anomalies on the east to indicate that alluvium is <100 m thick (S. Biehler, personal communication, 1998). Small squares on Figure 5 indicate where we consider basement to be within 100 m of the surface based on this. Note that because of complex geometry below the thrust fault, we refrained from using gravity data to constrain basement depth near its trace.

We contoured elevations of exposed weathered granite and buried basement of the footwall block at a scale of 1:62,500 and an interval of 200 ft (61 m). The resulting structure contour map shows a low (~3400 ft (~1.0 km)), smooth form (Figure 6). The smoothness results partly from the sparse data set used. The uncertainty in the elevation of basement represented by contours across basins is possibly as high as 20-30% (±100-200 m in most cases). There is additional uncertainty as to whether the basement is truly weathered granite and to what degree such a weathered surface is smooth and noneroded.

The structure contours of basement on the footwall block indicate that the surface topography of Lucerne Valley does not provide a good approximation of the elevation of the weathered surface. The contours show a nontrivial departure from topographic elevations and clearly define deep basins that have depressed bedrock. Alluvium in the trough-like basin north of the NFTS is as thick as 1.2 km and consists of debris derived primarily from the SBMs [*Sadler,* 1982]. The alluvium thins to negligible thicknesses east of the Helendale fault and eventually exposes weathered granite, where the footwall and hanging wall blocks meet at the eastern terminus of the NFTS. Several spurs and troughs are also apparent in the contours, where northwest trending faults of the eastern California shear zone have created small pressure horsts or grabens. Depression of basement by sediments, downwarp of basement along the NFTS, and the local displacement due to strike-slip faulting have considerably altered the geometry of the weathered surface of the footwall block from what was presumably once a smoother shape.

4. Structural Analysis

Figure 7 depicts a simplified structure contour map of the weathered surface both north and south of the NFTS. According to the above methods and assumptions, contours of the weathered surface approximate the present structural level of a smooth, preuplift horizon. This surface has been only insignificantly eroded during uplift of the SBMs. The widespread distribution and smoothness of surface remnants also suggest that the deeply weathered horizon was roughly uniform in elevation (i.e., low-relief) prior to deformation. The lack of sedimentologic evidence of pre-Pliocene relief argues that long-wavelength topographic features were absent prior to the recent uplift [*Sadler and Reeder,* 1983], while the contour construction method avoids minor undulations in the weathering front due to etching. Figure 7 should thus approximate rock uplift and subsidence relative to the low-relief paleotopography of the widespread weathered granite surface. Although we cannot be absolutely certain of the predeformational geometry of the weathered surface, our comparison of the relationship between its hanging wall and footwall position and the distribution of structures normalizes any effect of paleotopographic relief. We can thus use the weathered surface's constraint on rock uplift to study the tectonics of the thrust faults.

4.1. Displacement Along the Near-Surface NFTS and SAT

The geometry of structure contours along the Big Bear plateau bears a remarkable correspondence to the location of the NFTS (Figure 7). Elevations are low at either end but crest in the central segment of the thrust fault. On the eastern terminus of the thrust the weathered surface of the

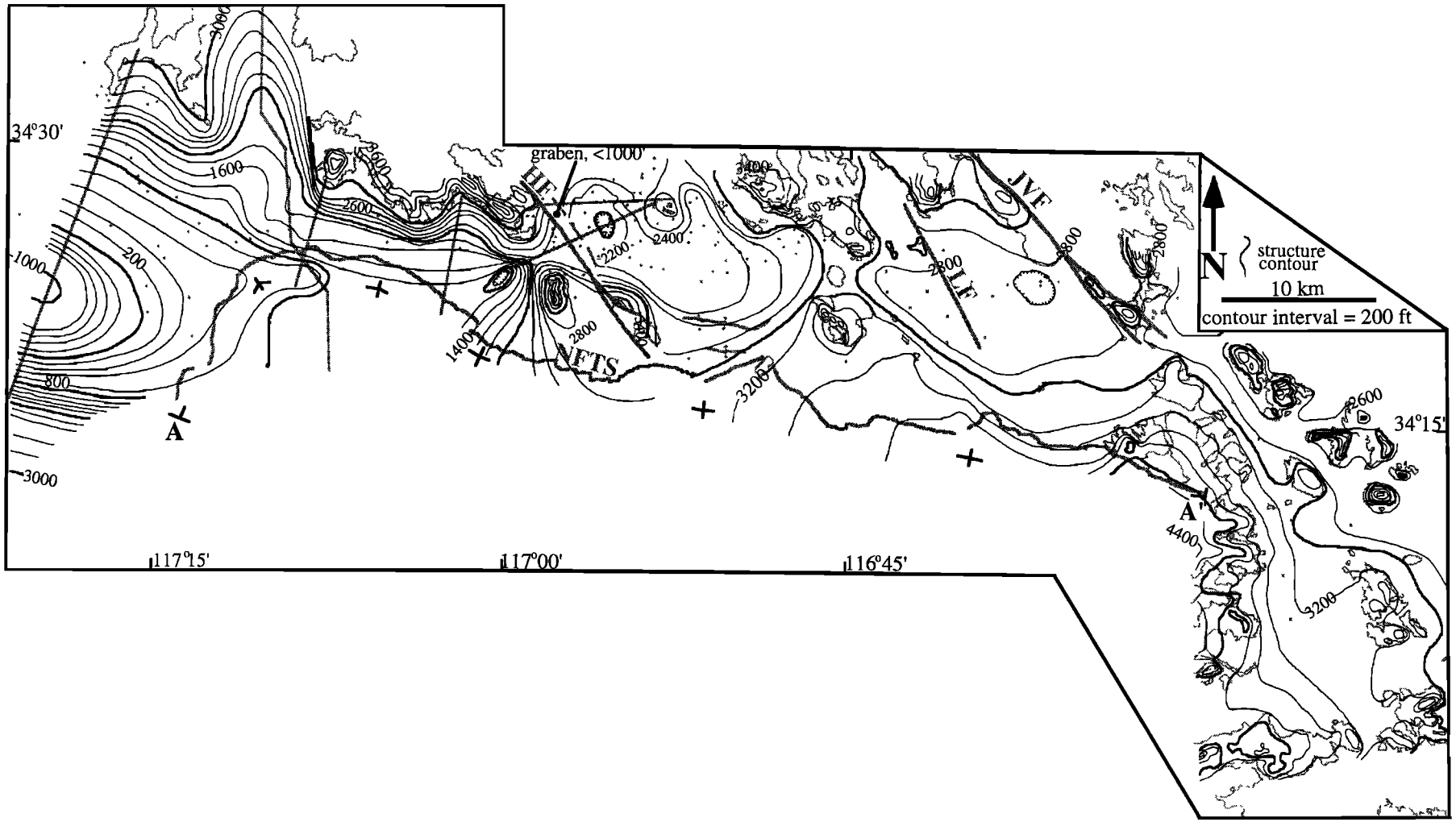

Figure 6. Structure-contour diagram of top of basement in the Mojave Desert shows elevation of the footwall block of the NFTS. Contour interval is 200 ft (61 m) with 1000 ft (304.8 m) index contours. The data used to construct this diagram (Figure 5) are shown by shading (lines of gravity and seismic profiles, boreholes, and outline of exposed basement). Major faults that disrupt the structure contours are also shown by shading (NFTS, North Frontal thrust system; HF, Helendale fault; LF, Lenwood fault; JVF, Johnson Valley fault).

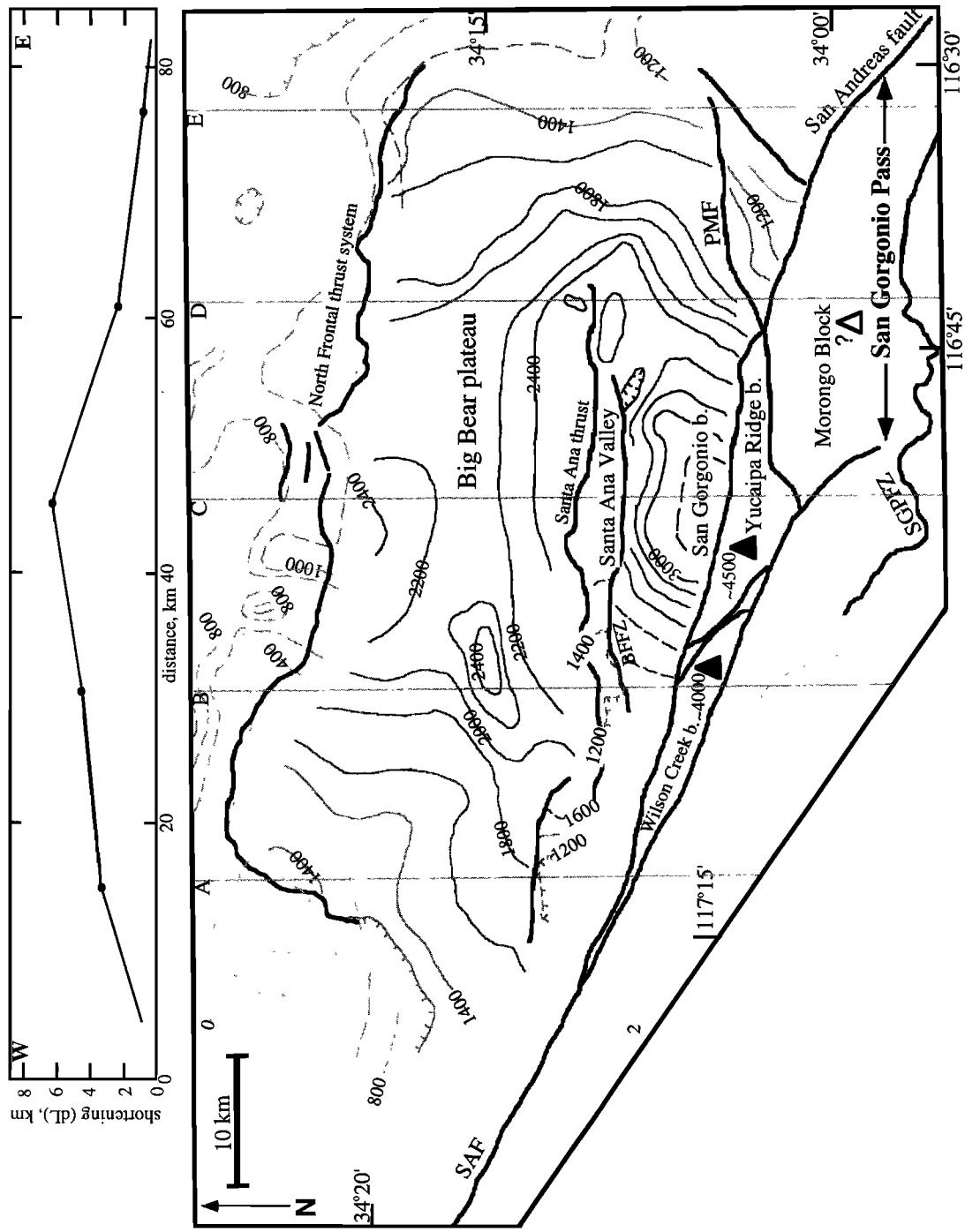

Figure 7. Simplified map of structure contours of the weathered surface atop the SBMs and granitic basement in the surrounding region showing the association of rock uplift with major structures. Contours are simplified versions of those in Figures 4 and 6. Contour interval is 200 m. The triangles atop the Wilson Creek and Yucaipa Ridge blocks indicate the inferred elevation those blocks would have if erosion were restored (based on evidence for their exhumation from radiometric helium ages [*Spotila et al.*, 1998]). Such a constraint does not exist for the Morongo block. The upper plot of horizontal shortening along each profile is based on Figure 12. BFFZ, Barton Flats fault zone; SGPFZ, San Gorgonio Pass fault zone.

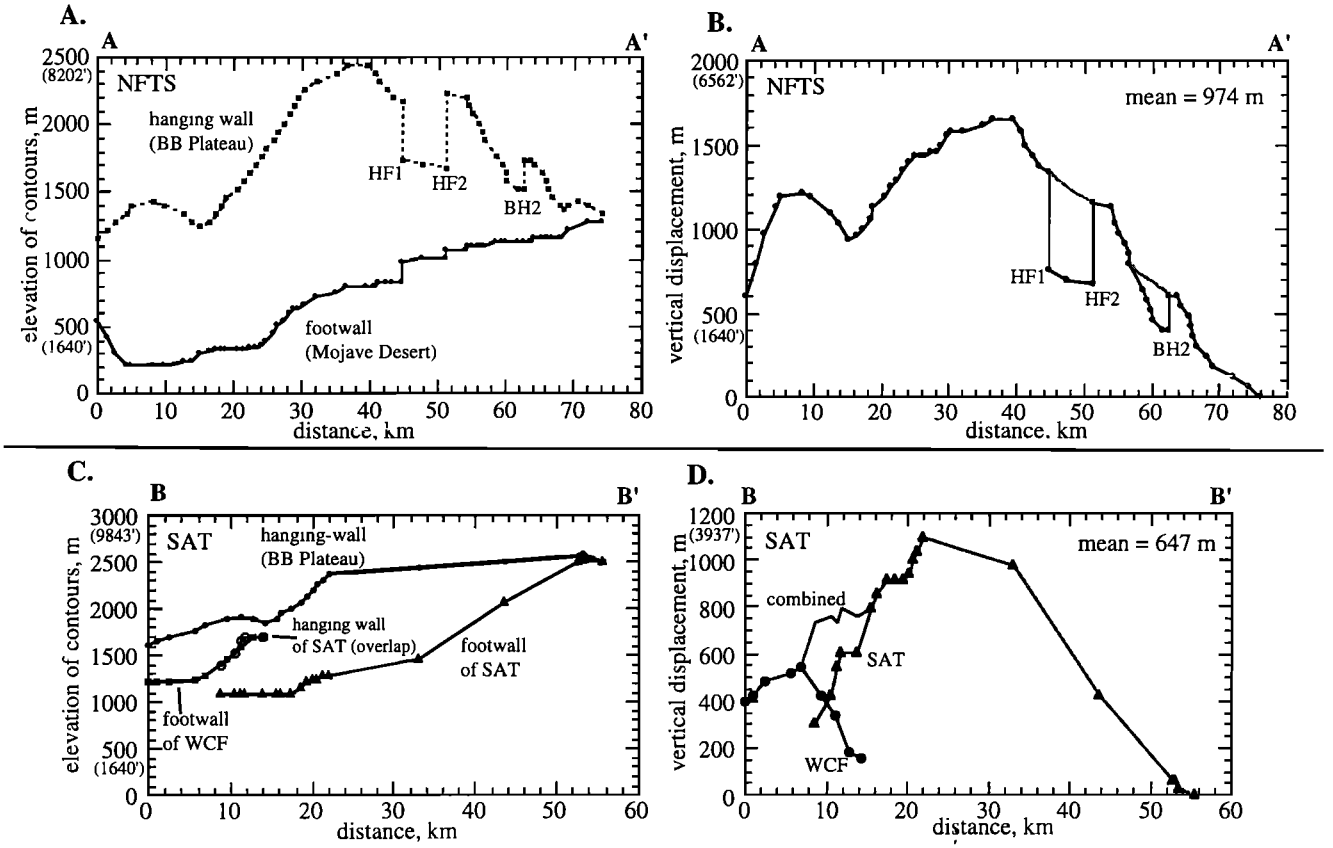

Figure 8. Vertical displacement along the NFTS and SAT, which equals the difference in weathered surface elevations atop hanging wall and footwall blocks. (a) Comparison of structure contour elevations atop the Big Bear plateau and Mojave Desert adjacent to the surface trace of the NFTS (along line AA'; see Figures 4 and 6). HF1 and HF2 are strands of the Helendale fault that bound the Helendale graben; BH2 is a strand of the Bighorn fault zone. (b) The difference between the hanging wall and footwall elevations along AA', which equals the vertical displacement along the NFTS. (c) Comparison of structure contour elevations atop the plateau and Santa Ana Valley adjacent to the surface trace of the SAT (along line BB'; see Figure 4). Note that the footwall elevations are different for the Waterman Canyon fault and the main SAT strand. Where the two strands overlap, the elevations of the hanging wall for the main SAT strand were taken as the elevation of the footwall to the Waterman Canyon fault. (d) The difference between the hanging wall and footwall elevations along BB', which equals the vertical displacement along the SAT. Solid circles represent displacement on the Waterman Canyon fault, whereas solid triangles represent displacement on the main strand of the SAT. The line above represents the sum of these two.

footwall and hanging wall blocks actually merge. This pattern strongly suggests that the NFTS has vertically displaced a surface that was previously nearly level. By subtracting the elevation of contours atop the hanging wall and footwall blocks we have directly measured the magnitude of this vertical displacement. This measurement is not dependent on assumptions about the original geometry of the surface.

Because the structure contours of the weathered surface in the footwall block are lower in elevation than present topography, the resulting plot of vertical displacement along the NFTS is greater than the height of the fault escarpment (Figures 8a and 8b). Vertical displacement peaks near the center of the fault trace (1650 m) but drops toward each side to resemble a smooth, quasi-parabolic distribution. Displacement drops to zero on the east but lingers with moderate magnitude (~610 m) west of the NFTS. This is because the NFTS terminates within the Miocene Squaw Peak thrust system, which locally offsets the weathered surface [*Meisling and Weldon,* 1989] (Figure 2). Other complexities in the displacement profile also occur where different fault segments are encountered. Grabens between strands of the Helendale fault and Bighorn fault zones, for example, down-drop the weathered surface of the hanging wall block (Figures 2 and 4). Lack of data prevents seeing a similar down-drop in the footwall block (Figures 5 and 6), but if it exists, the displacement profile should extend smoothly across these grabens (shaded line

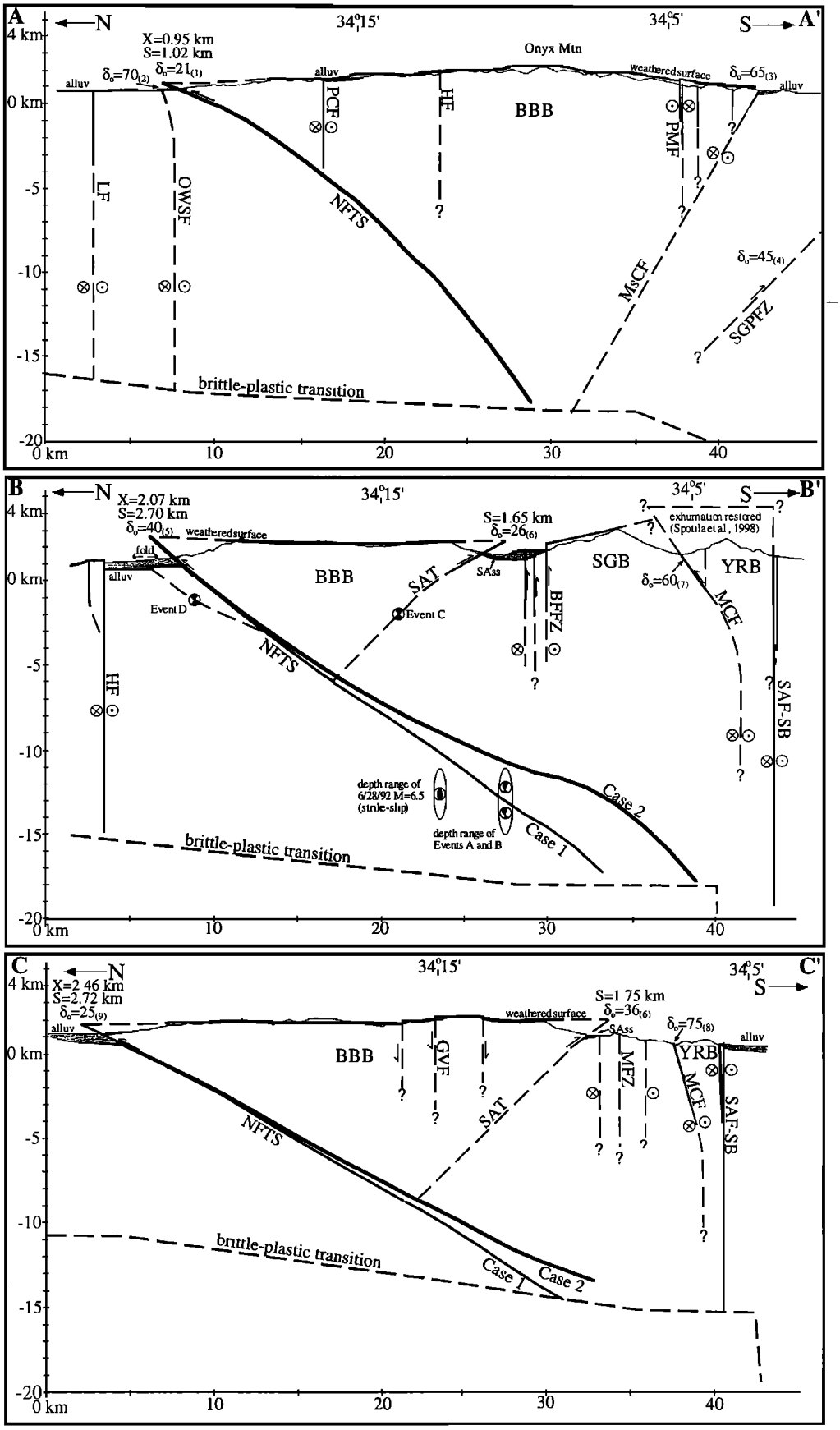
A
N
34°15'
34°05'
S
A'
4 km
0 km
-5
-10
-15
-20
X=0.95 km
S=1.02 km
δo=70(2)
δo=21(1)
alluv
Onyx Mtn
weathered surface
δo=65(3)
PCF
HF
BBB
PMF
LF
OWSF
NFTS
MsCF
δo=45(4)
SGPFZ
brittle-plastic transition
0 km
10
20
30
40
B
N
X=2.07 km
S=2.70 km
δo=40(5)
weathered surface
fold
alluv
34°15'
34°05'
S
B'
exhumation restored (Spotila et al., 1998)
S=1.65 km
δo=26(6)
BBB
SAT
SAss
SGB
YRB
δo=60(7)
Event D
Event C
BFFZ
MCF
HF
NFTS
SAF-SB
depth range of 6/28/92 M=6.5 (strike-slip)
depth range of Events A and B
Case 2
Case 1
brittle-plastic transition
C
N
34°15'
34°05'
S
C'
X=2 46 km
S=2.72 km
δo=25(9)
alluv
S=1 75 km
δo=36(6)
weathered surface
SAss
δo=75(8)
BBB
GVF
SAT
MFZ
YRB
MCF
SAF-SB
NFTS
brittle-plastic transition
Case 1
Case 2

Figure 9.

in Figure 8b). Owing to the general limits in data that define contour elevations the entire displacement plot probably has an inherent uncertainty of a few hundred meters (~10-15%).

We measured vertical displacement along the SAT in a similar manner, but several complications resulted in a larger uncertainty than along the NFTS. The weathered surface is locally not exposed along the southern footwall, owing to burial by thick fanglomerates of Santa Ana Valley on the east, where no data constrained the depth to basement. The weathered surface has also been locally removed by erosion on the west, where the SAT outcrops midway up the southwestern escarpment of the plateau (Figure 4). Another complication is the Waterman Canyon fault on the west, which shares the SAT's trend, position on the escarpment, and sense of separation. This fault may represent a westward continuation of the SAT, implying that its displacement be summed with the SAT. We thus measured the displacement along the southern thrust faults by differencing the elevation of structure contours of the hanging-wall block with those of the footwall blocks of both the SAT and Waterman Canyon fault separately (Figure 8c). Where not exposed, the elevation of the weathered surface of the footwall was approximated as the elevation of the surface trace of the thrust fault itself. The resulting combined displacement profile for the two faults reveals a bell-shaped curve that is similar to the NFTS profile (Figure 8d). The maximum vertical offset along the SAT is 1100 m, but displacement averages ~650 m. The uncertainty of the displacement values are probably as great as 25% (~200 m).

4.2. Subsurface Geometry of the NFTS and SAT

The geometry of structure contours of the weathered surface are clearly associated with the bounding thrust faults (Figure 7). The along-strike increase in contour elevations toward the center of the plateau represents an increase in displacement along the faults from their eastern and western terminations. Cross-strike changes (north to south) may instead represent downdip variations in thrust fault dip. The contour pattern is similar to the geodetically observed coseismic vertical displacements for individual ruptures of thrust faults [e.g., *Savage and Hastie,* 1966], which can be used to define fault dip at depth. We use the structure contours similarly to explore subsurface geometry of the NFTS and SAT in three north-south cross sections (Figure 9).

The antithetic symmetry of the NFTS and SAT has previously inspired the hypothesis that the subsurface structure of the range is shaped like a flower or mushroom, in which low-angle faults near the surface steepen to a vertical zone at depth [*Sadler,* 1982]. However, we have several reasons to propose that the NFTS undercuts the SAT. The SAT is the lesser of the two faults, having significantly less vertical offset and shorter length (Figures 2 and 8). Although the SAT has uplifted the plateau above the Santa Ana Valley, the valley disappears within a high-elevation bulge in structure contours to the east (Onyx Mountain; Figure 7). Because the topographic expression of the SAT is lost there as well, it cannot have contributed to the uplift of this bulge. Similarly, the trace of the SAT itself appears to have been uplifted, rising eastward to over 2.5 km elevation. This implies that the NFTS undercuts the SAT, uplifting the secondary thrust fault along with the plateau itself. The high contours atop the San Gorgonio block further imply that the NFTS penetrates the crust south of the SAT. Rather than merging into a high-angle fault system midway beneath the plateau, the NFTS may thus extend southward to the San Andreas fault. We focus our analysis to constrain the geometry of the NFTS, the more important structure.

However, the area of the weathered surface underlain by the SAT has experienced deformation due to both thrust faults. To learn about the geometry of the NFTS, we must first remove the vertical displacement produced by the SAT. We attribute a fixed component of vertical displacement to the SAT, using two end-member scenarios. In the first case, we assume that the entire hanging wall block has a uniform vertical displacement,

Figure 9. Shape of the NFTS in north-south cross sections across the SBMs (AA' is at 116°40'W, BB' is at 116°55'W, and CC' is at 117°05'W; locations are shown in Figure 2), on the basis of the deformation of the weathered surface. Topography is shown as an irregular light line without vertical exaggeration. The dark line near the surface topography represents the elevations of the weathered surface (w.s.) from structure contours (dashed where inferred). Orientation of the NFTS is based on analysis described in the text. Displacements at the trace of each thrust are listed (S, net slip; X, horizontal component). Fault orientations at the surface are labeled (δ_0) and referenced with subscripts (1, *Miller* [1987]; 2, *Dibblee* [1967b]; 3, *Dibblee* [1967a]; 4, *Jones et al.* [1986]; 5, *Rzonca and Clark* [1982]; 6, *Jacobs* [1982]; 7, *Allen* [1957]; 8, *Dibblee* [1974]; 9, *Li et al.* [1992]). Other data are from *Sadler* [1993] and *Dibblee* [1964a, b]. Faults are dashed where orientation is inferred, and fault type is indicated by arrows (vertical motion) or circles (circle with cross indicates lateral motion away; circle with dot indicates lateral motion toward). Focal mechanisms from Figure 11 are given as upper hemisphere plots projected onto the perspective plane of section BB' (e.g., events A-D represent thrust motion). MB, Morongo block; MCF, Mill Creek fault; MFZ, Mentone fault zone; MsCF, Mission Creek fault; OWSF, Old Woman Springs fault; OWss, Old Woman Sandstone; SAF-SB, San Bernardino strand of the San Andreas fault; SAss, Santa Ana sandstone; SAV, Santa Ana Valley; YRB, Yucaipa Ridge block (other abbreviations are as in Figures 2, 4, 6, and 7).

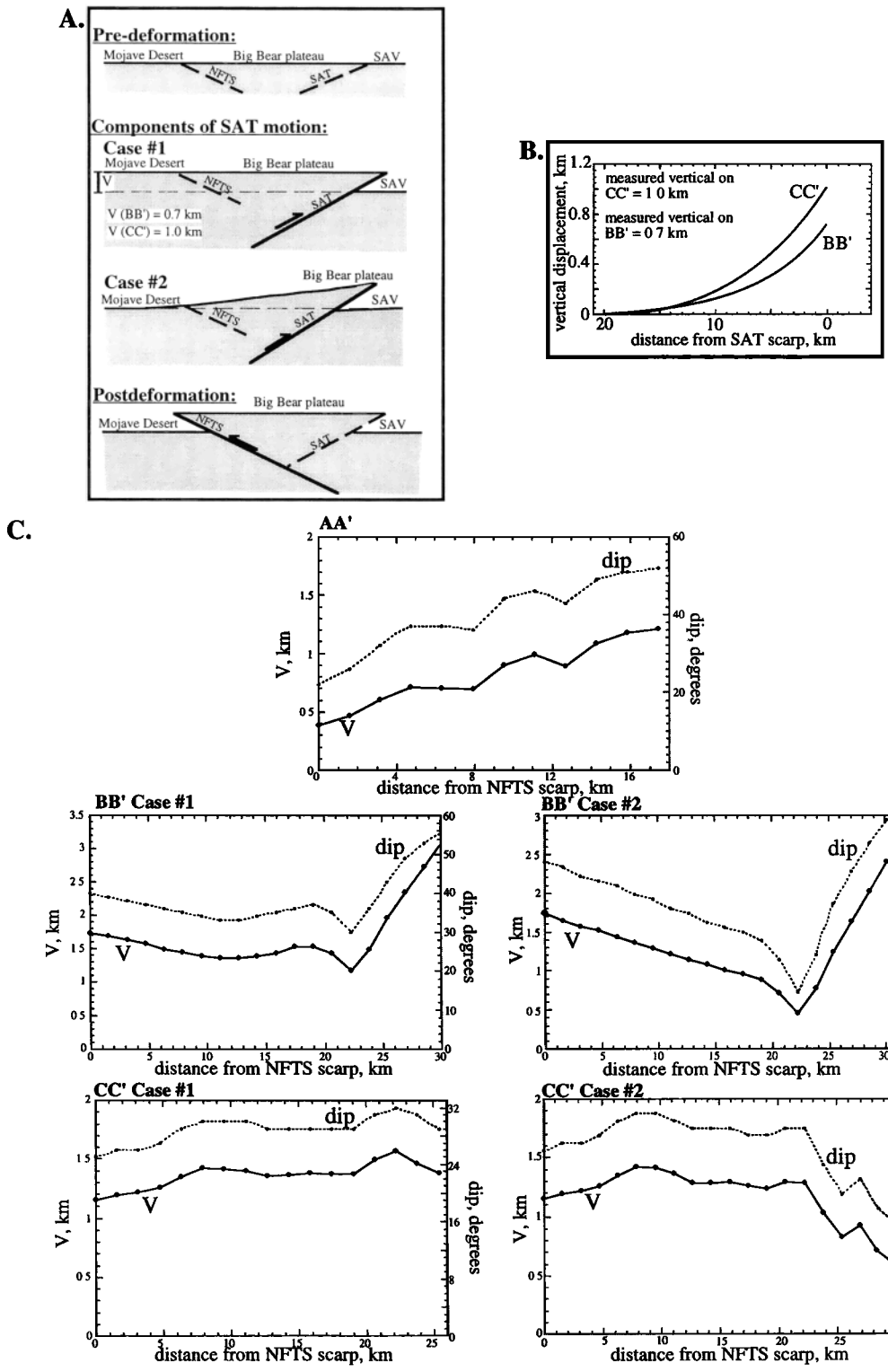
A.
Pre-deformation:
Mojave Desert
Big Bear plateau
SAV
NFTS
SAT
Components of SAT motion:
Case #1
V
V (BB') = 0.7 km
V (CC') = 1.0 km
Case #2
Postdeformation:
B.
vertical displacement, km
measured vertical on CC' = 1 0 km
measured vertical on BB' = 0 7 km
CC'
BB'
distance from SAT scarp, km
C.
AA'
dip
V
V, km
dip, degrees
distance from NFTS scarp, km
BB' Case #1
BB' Case #2
CC' Case #1
CC' Case #2

Figure 10.

equal to the value measured at the surface trace of the SAT (Figure 10a). Both the plateau and Mojave Desert would have thus been uplifted the same amount relative to the Santa Ana Valley. Given that the NFTS has uplifted the plateau and Santa Ana Valley relative to the Mojave Desert, no vertical displacement attributable to the SAT must be removed prior to analyzing the orientation of the NFTS.

In the second case, we assume that vertical deformation due to SAT motion decays with distance northward away from the fault surface trace (Figure 10a). Because vertical elastic displacements associated with individual earthquakes are confined to narrow zones near faults [e.g., *Savage and Hastie,* 1966], it is plausible that the long-term deformation associated with the SAT has been similarly limited to a fixed distance from its surface trace. This requires that a component of plateau uplift be subtracted prior to analyzing structure contour elevations to learn about NFTS geometry. To maximize the difference between our two cases, we assume that deformation associated with the SAT is confined to a narrow distance from the fault. This results in significant reduction of vertical displacement associated with the NFTS in the southernmost Big Bear plateau, while not affecting that associated with the NFTS in the northern plateau (Figure 10a). *King et al.* [1988] have shown that the width (i.e., normal to strike) of long-term deformation associated with dipping faults, although greater than the width of coseismic elastic deformation, is highly dependent on the flexural rigidity of the crust and the degree of erosion and sedimentation. It is most narrow when postseismic stress relaxation of the crust is minimized by a thin apparent elastic thickness and minimal isostatic adjustment (i.e., no erosion). Figure 10b shows how vertical displacement should decrease away from the SAT surface trace, based on the results of *King et al.* [1988] for an uneroded, 45° dipping reverse fault that penetrates a 15-km-thick brittle crust with an apparent elastic thickness of ~4 km. We subtract these components of vertical displacement from elevations of structure contours on both cross sections prior to analysis of NFTS geometry.

To use elevations of structure contours to learn about the shape of the NFTS, several more assumptions are required. On the basis of available geologic data we assume that the weathered granite surface was approximately horizontal prior to uplift. The paleogeography of the region is not uniquely constrained, however, and this assumption represents the weakest aspect of our analysis. We also assume that horizontal components of thrust motion at depth do not vary significantly from surface measurements. This assumption is well founded if convergence is associated with far-field, purely horizontal translation of plates along the San Andreas fault. Along-strike variations in slip exist along the NFTS as a function of eastern and western fault terminations (e.g., Figure 8), but we do not attribute these to cross-strike changes in fault orientation. Last, we assume that deformation of the weathered surface was produced primarily by the NFTS and SAT. The San Andreas fault and secondary reverse faults may have deformed the weathered surface in the westernmost SBMs (e.g., western San Bernardino arch [*Meisling and Weldon,* 1989]), but elsewhere it is clear that the thrust faults have been the main structures responsible for uplift.

Given these assumptions, variation in the elevation of structure contours should reflect the orientation of the underlying thrust faults. Higher regions should indicate greater vertical components of fault motion, in turn implying steeper underlying fault dips. Lower elevations instead imply more shallow dips. This represents a space balance approach to constraining downdip changes in thrust fault geometry. The specific constraints used for the subsurface orientation of faults are described below.

4.2.1. Constraints on fault geometry. We constructed cross sections using a 1:62,500 scale topographic base and elevations of the weathered surface from the contour maps (Figures 4 and 6). The elevation of basement in the San Bernardino Valley on section CC' is from *Willingham* [1981]. The magnitude of rock uplift for southern fault blocks is based on thermochronometry [*Spotila et al.,* 1998]. Fault location and orientation observed at the surface were boundary conditions for cross-

Figure 10. The dip of the NFTS in cross sections based on changes in elevation of structure contours away from the surface trace of the thrust. To make this calculation, the component of vertical displacement attributable to the SAT must be removed. (a) Schematic diagram showing two plausible cases of vertical deformation on the SAT. In case 1, slip does not decrease with distance northward from the SAT's trace, so that the plateau and Mojave Desert are displaced equally relative to the Santa Ana Valley (SAV). This case does not require any displacement of the weathered surface between plateau and Mojave Desert to be removed prior to the NFTS dip analysis. In case 2, slip decreases away from the SAT, so that a correction must be made prior to calculation of NFTS dip. (b) Plots of the decay in vertical displacement attributed to the SAT on cross sections BB' and CC' for case 2, based on a model of long-term elastic deformation and stress relaxation for a 45° dipping reverse fault in a 15-km-thick brittle crust with a 4-km-thick apparent elastic thickness [*King et al.,* 1988]. This displacement was subtracted from plateau elevations prior to analysis of NFTS dip. (c) Plots of the elevation of structure contours (V) as a function of distance from the NFTS for each cross section. Results for both cases of assumed SAT deformation are shown. Differences between these elevations and the elevation directly above the NFTS scarp are taken as indications of dip changes at depth, as $V/X = \tan\delta$ (δ is dip and X is constant horizontal shortening). Resulting values of dip are plotted as well.

section construction (as referenced; Figure 9). Faults for which no subsurface information is available were simply projected to the base of the brittle crust at their near-surface attitude. This is the case for most of the strike-slip faults in the sections. For many high-angle faults, there were no data available on surface orientation other than topographic expression [cf. *Spotila,* 1999]. These are drawn vertically, so that faults with dip-slip motion are not inferred to be normal or reverse (Barton Flats and Green Valley fault zones).

We determined the orientation of the NFTS using the elevation of structure contours and the displacements measured along its surface trace. Apparent net slip S along the trace of the NFTS was measured by projecting the fault upward to intersect the projection of the weathered surface north of the escarpment (Figure 9). The weathered surface is unlikely to bend downward as a fold at the escarpments, given that thermochronometric isochrons remain nearly horizontal at both the northern and southern margins of the plateau [*Spotila et al.,* 1998]. The horizontal component X of apparent net slip S was used as a fixed boundary condition for the determination of downdip fault orientation in each cross section. The elevations of the weathered surface V were plotted away from the NFTS on each cross section at ~1.5 km intervals (Figure 10c). We determined fault dip below (δ) as $V/X = \tan(\delta)$. Resulting dips were plotted sequentially downward for each vertical offset measured but were offset from where calculated by a distance equal to the horizontal component of motion (to account for vergence). Small high-angle faults with minor vertical separation of the weathered surface (Barton Flats and Green Valley fault zones) were backslipped prior to calculating thrust fault dip. This was completed for the two cases of prescribed SAT displacements (lines A and B; Figures 9 and 10a). Note that this space balance technique was used rather than an elastic model because of the insensitivity of such models to fault dip and their dependence on mechanical assumptions [e.g., *King et al.,* 1988].

Seismicity is often used to constrain the subsurface orientation of faults but provides only minor constraint on our cross sections. Recent seismicity beneath the SBMs is dominated by aftershock clusters along the strike-slip ruptures of the 1992 Landers-Big Bear sequence [*Hauksson et al.,* 1993; *Jones and Hough,* 1995] and the oblique slip 1986 Palm Springs rupture [*Jones et al.,* 1986] (Figure 11). The 1986 event defines a 45°N dip for the San Gorgonio Pass fault zone (AA'; Figures 9 and 11). Most faults, including the NFTS and San Andreas, cannot be defined by hypocenters. A few diffuse clusters of small 1992 aftershocks occur near the NFTS (AA' and BB'), but these probably represent secondary deformation within the footwall. Several moderate events with thrust-type focal mechanisms occurred along the NFTS and SAT in 1992 [*Hauksson et al.,* 1993; *Jones and Hough,* 1995]. Two of these occurred deep along the projection of the NFTS (events A and B; BB'), but defining the orientation of the NFTS based on these is tenuous. Event C is a 45°S thrust rupture that occurred near the SAT (section BB'). We have steepened the SAT from its 26° and 36°S surface dips to intersect this 45°S plane (BB' and CC'). A fourth thrust rupture occurred at 2.6 km depth near the NFTS trace (event D; BB'). This was associated with displacements visible on synthetic aperture radar interferograms [*Feigl et al.,* 1995]. This rupture dipped 28 ± 4°S based on an elastic dislocation model of its displacement but may have occurred on a secondary blind thrust responsible for folding north of the main trace [*Spotila,* 1999; *Miller,* 1987; *Dibblee,* 1964b]. The depth distribution of recent seismicity also delineates the brittle-plastic transition beneath the SBMs (Figures 9 and 11). This rheological boundary marks the lower limit to which brittle faults are projected. Our geometry for this is similar to that in previous reports [*Corbett,* 1984; *Magistrale and Sanders,* 1996].

4.2.2. Resulting cross sections. Because cross section AA' cuts the plateau east of the SAT's apparent termination, none of the weathered surface's vertical displacement had to be restored prior to performing analysis of NFTS geometry. The weathered surface rises steadily to the south, away from the surface trace of the NFTS. This requires the NFTS to steepen downdip in our analysis (Figure 9a). The distinctly convex NFTS steepens to a dip of 52°S before it intersects the brittle-plastic transition at ~18 km depth. The vertical displacement of the weathered surface, however, continues to rise south of the NFTS's intersection with the brittle-plastic transition, beyond where elastic deformation would be expected to occur. To extend the NFTS farther south beneath the rise of Onyx Mountain, we envision that it could merge with the mechanical discontinuity at the base of brittle crust to form a detachment. In this case, the bulge in the weathered surface could result from internal deformation (i.e., kink band migration) associated with the bend between the detachment (i.e., flat) and the steeply dipping NFTS (i.e., ramp). Alternatively, the bulge could have been produced by the steeply north dipping Mission Creek fault, although this strand of the San Andreas fault zone does not have significant vertical motion along its trace.

The weathered surface in cross section BB' is deformed by both thrust faults, and thus we backslipped the SAT prior to analyzing geometry of the NFTS (Figure 9b). In one scenario we assumed motion on the SAT does not decrease northward from its trace, as shown in Figure 10 (Case 1). Given this assumption, the NFTS flattens slightly (to 30°) until ~14-km depth, where it steepens (to 49°) to account for uplift of the San Gorgonio block. However, the fault meets the brittle-plastic transition north of the high part of this southern block. It is thus not clear that the NFTS can explain the San Gorgonio block uplift in this case. In the second case, motion on the SAT is assumed to decrease away from its trace (Case 2; Figure 10). This means that a significant fraction of the weathered surface's deformation is removed and results in pronounced, listric-like flattening (to 12°) of the NFTS. The fault remains above the brittle-plastic transition beneath the entire San Gorgonio block, where it steepens to account for the localized uplift. This case suggests the NFTS can explain the uplift of this southern block (with the help of

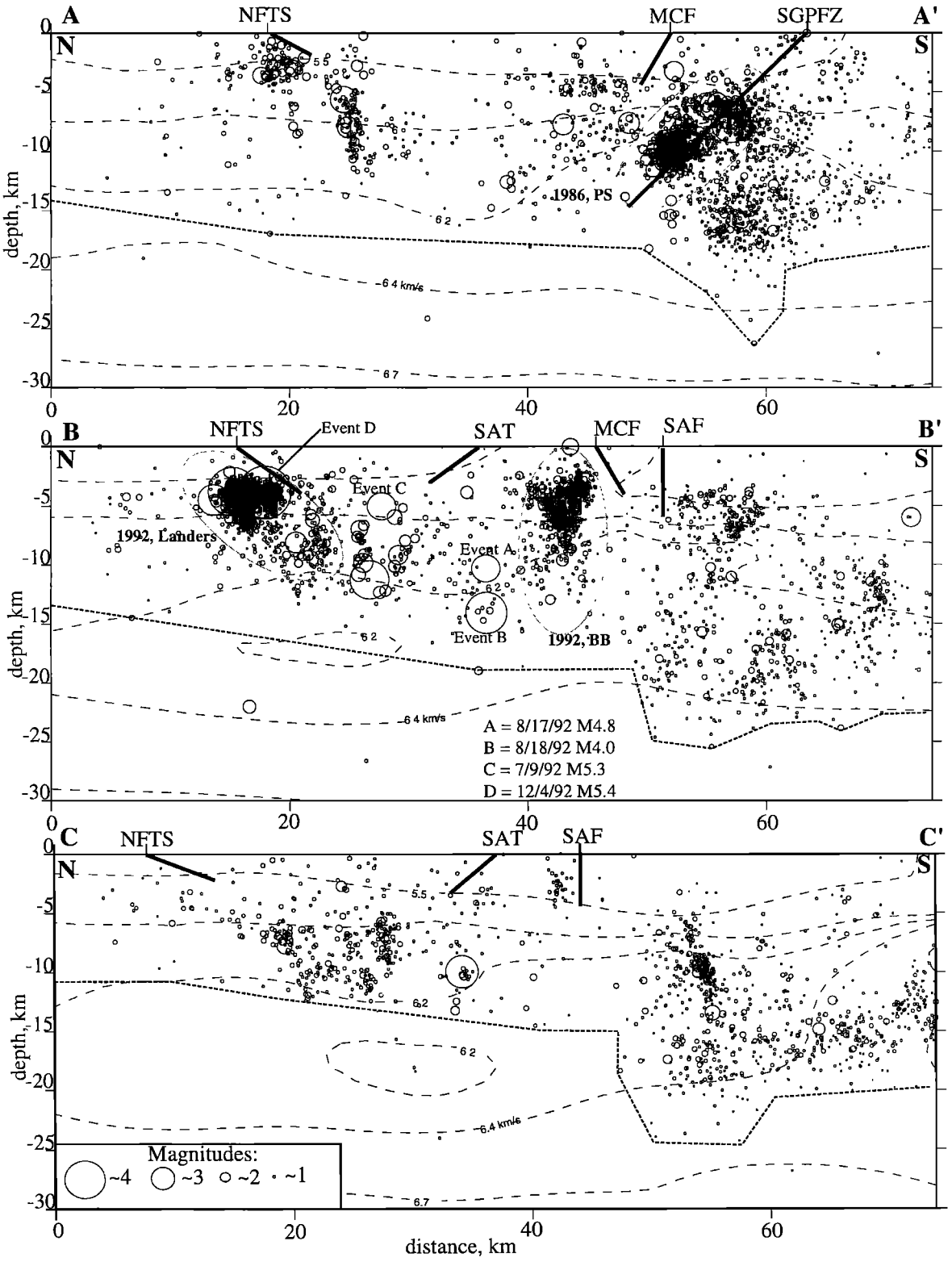

Figure 11. Seismicity constraining the extent of brittle crust and the geometry of some faults beneath the SBMs. North-south cross sections AA', BB', and CC' depict earthquakes from 1981-1998 from within the boxes shown on Figure 2 (data are from E. Hauksson, manuscript in preparation, 1999). Event locations are based on the velocity structure shown by the labeled thin dashed lines (km/s). The thick dashed line represents the brittle-plastic transition, inferred to equal the base of seismicity. Focal mechanisms of events A-D appear on Figure 9. Events A and C actually occur outside of the window of BB' shown on Figure 2 but are projected onto the plot from several kilometers east [*Jones and Hough,* 1995]. Clusters of events are labeled (PS, Palm Springs; BB, Big Bear). Locations and near-surface orientations of major faults are shown. MCF, Mill Creek fault; NFTS, North Frontal thrust system; SAF, San Andreas fault; SAT, Santa Ana thrust; SGPFZ, San Gorgonio Pass fault zone.

the Barton Flats fault zone). We consider this second scenario to be more realistic, given that displacement along the SAT probably decreased away from its trace. In neither case can the NFTS account for the major rock uplift of crustal slivers south of the San Gorgonio block [*Spotila et al.*, 1998].

A less complicated NFTS geometry results from the analysis along cross section CC' (Figure 9c). In the first case of SAT motion (Figure 10) the NFTS steepens slightly with depth (25° to 32°) to explain a slight rise in the weathered surface near Butler Peak. This steepening is less apparent in the second case, in which the NFTS flattens (to 15°S) because of the share of vertical displacement attributed to the SAT (Figure 10). This represents a minor difference, however, and the NFTS and SAT can adequately explain the uplift of the plateau in both cases.

The geometry of the NFTS implied in each of these three cross sections is very different. Section BB' reveals a contorted shape, because of the complexity in the weathered surface across the plateau, low Santa Ana Valley, and high San Gorgonio block. Sections AA' and CC' imply opposite geometries (convex on the east, listric on the west) because the SAT accounts for some uplift on the west but none on the east. According to this analysis, however, displacement along the NFTS and minor motion on the SAT (and Barton Flats fault zone) can adequately account for deformation of the weathered surface across the entire Big Bear plateau and San Gorgonio block. Although our structural analysis is nonunique and limited by the assumptions we have made, it thus provides a plausible explanation for the shape of structures beneath the range.

4.3. Horizontal Shortening in the SBMs

Although the weathered surface places valuable new constraints on the uplift of the Big Bear plateau, the thrust faults bounding the plateau are not the only transpressive deformation in the SBMs. Fault blocks in the southern part of the range have experienced major rock uplift and exhumation due to oblique slip on high-angle structures [*Spotila et al.*, 1998] (Figure 2). Horizontal plate motion in the SBMs is thus accommodated by a variety of mechanisms. To learn about the cause of transpressive uplift in the SBMs, we must first summarize the pattern of convergence represented by the structural relief of the entire range.

The horizontal plate motion that has been accommodated by uplift of the SBMs can be estimated by simple volume balance. The weathered surface provides a constraint on the magnitude of rock uplift across much of the range, whereas the minimum rock uplift and erosion for blocks in the south can be inferred from radiogenic helium thermochronometry [*Spotila et al.*, 1998]. By restoring the volume eroded from each block a paleotopographic surface is approximated that can be restored to constrain the magnitude of horizontal shortening. We have done this for five north-south profiles in Figure 12. Similar to the cross-section analysis presented above, the erosion near thrust fault escarpments is restored by projecting the weathered surface to intersect the upward projection of each thrust plane. For the thermochronometry, the preerosion elevation of each block is restored and extended horizontally in either direction to the projection of bounding faults. The resulting estimate of the paleotopographic surface is thus a discontinuous line across each profile. By assuming this was approximately horizontal prior to deformation and uplift of the SBMs, this line can be straightened to estimate the horizontal shortening (change in line length dL) for each profile. These estimates are less precise than the measurement of horizontal motion along individual faults in cross section but provide constraint on how horizontal motion is distributed across the entire range. Uncertainty in these values is difficult to assess and most dependent on whether fault projections are valid, the original horizontality of the topography, and whether significant internal deformation has occurred in the heavily eroded southern blocks.

The largest estimated value of horizontal shortening occurs in the center of the range, just northwest of the restraining bend in the San Andreas fault at San Gorgonio Pass (profile C, dL = 6.3 km). This represents a minimum estimate of the total shortening in the SBMs, given that the thermochronometric constraints provide minimum values of rock uplift and do not account for internal deformation. This convergence resolves to a N37°W component of ~5 km, which is 5% of the total Pacific-North American motion since 2 Ma [*DeMets*, 1995]. To the east and west, convergence decreases smoothly, as shown in the upper part of Figure 7. The resulting distribution is similar to how slip varies along the NFTS and SAT (Figure 8). On the basis of these profiles, we estimate the total volume of rock uplifted during construction of the SBMs to be ~4400 km^3 (Figure 12). The magnitude of erosion is also evident on these profiles and is greatest on the thrust fault escarpments and southernmost fault blocks. The total volume eroded from the range is ~1200 km^3, which should fit into the deep alluvial basins in the surrounding region (Figure 12). The average incision depth along each profile, calculated as the quotient of the eroded area and the profile width, varies from 0.16 to 0.71 km (Figure 12). These estimates imply a whole-mountain average incision of 0.39 km, corresponding to an average erosion rate of ~0.16 mm/yr (assuming ca. 2.5 Ma initiation of uplift [*May and Repenning*, 1982]). This is slightly lower than for other active mountains in California (e.g., ~0.2-0.3 mm/yr, Santa Cruz Mountains [*Anderson*, 1990], ~0.5 mm/yr, Santa Monica Mountains [*Meigs et al.*, 1999]).

5. Discussions

5.1. Displacements Along Thrust Faults

Both the NFTS and SAT exhibit large vertical displacements in the SBMs (Figure 8). Given their gentle dips, the net displacements along these faults are even larger (Figure 9). Using maximum vertical offset and

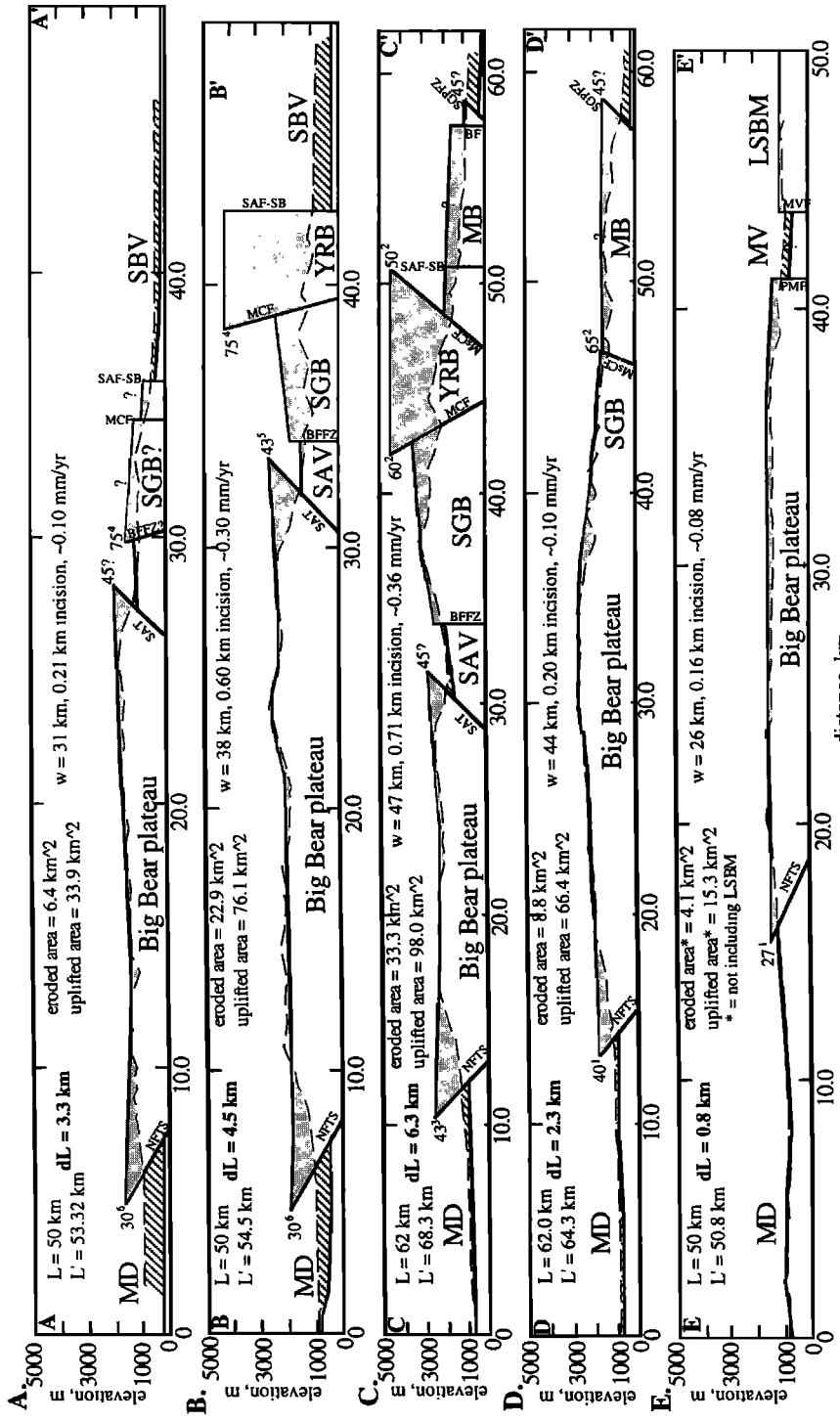

Figure 12. North-south profiles across fault blocks whose magnitude of exhumation are constrained by the weathered surface and thermochronometry, which enable calculation of horizontal shortening across the SBMs (A-E in Figure 7). The thin dashed line represents present topography without vertical exaggeration. The thick solid line represents either the weathered surface or topography restored based on thermochronometry [*Spotila et al.*, 1998]. Horizontal shortening (*dL*) is the difference in horizontal length of each profile (*L*) and the total length of the heavy solid line (*L'*). Shortening reaches ~6 km in the center of the range and diminishes to either side, as plotted in Figure 7. Erosion can also be calculated from these profiles. The gray shaded pattern indicates the area removed by erosion, which is summed in each profile. Average incision for each profile is the eroded area divided by profile width *w*. Incision rates are for the past 2 Myr. The ruled pattern indicates where deposition has buried the weathered surface. The area uplifted in each profile is relative to a base level defined by the elevation of basement north and south of the uplifted region. The total uplifted volume of the range is the sum of the products of uplifted area and the distance between profiles (15.3 km). Fault dips for projections are shown with superscripts that refer to the following: 1, *Miller* [1987]; 2, *Allen* [1957]; 3, *Rzonca and Clark* [1982]; 4, *Dibblee* [1974]; 5, *Jacobs* [1982]; 6, *Li et al.* [1992]. Abbreviations are as in Figures 2 and 9; BF, Banning fault; LSBM, Little San Bernardino Mountains; MV, Morongo Valley; MVF, Morongo Valley fault; SBV, San Bernardino Valley.

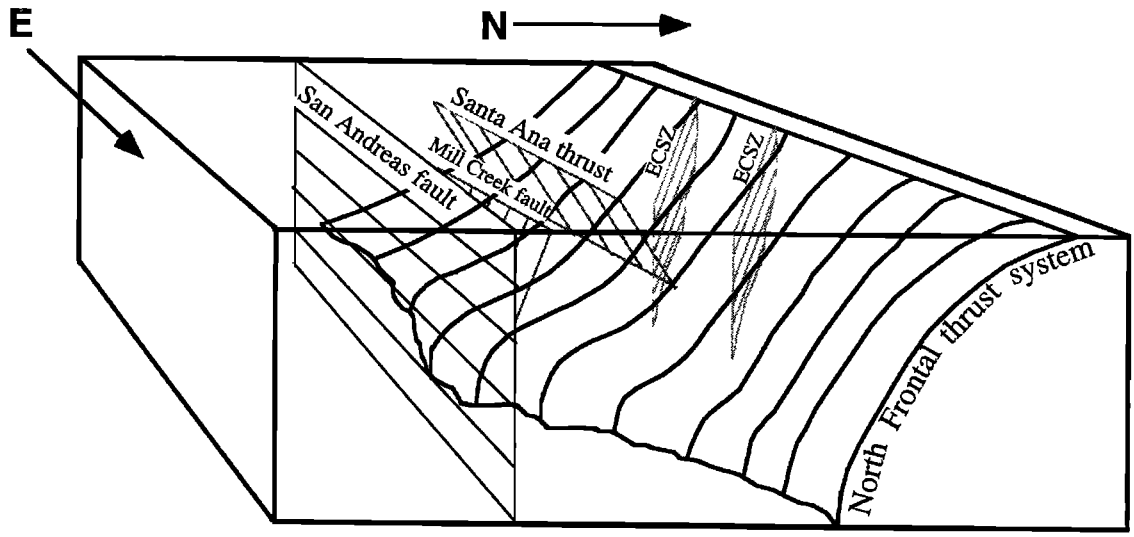

Figure 13. Schematic block diagram of the primary structural architecture of deformation in the SBMs inferred from our analysis of the weathered surface. The NFTS is shown with a contorted geometry that includes both convex and concave portions. The SAT appears as a simple, planar thrust. The dextral faults of the eastern California shear zone are shown as penetrating the upper plate of the thrust faults to indicate the possibility that both have been active during uplift of the range. Although this diagram is schematic and only represents our best guess for the structural geometry of the range, it gives a sense of the complexity and variability of transpressional deformation in the SBMs.

average dip orientation for each fault (35°S, NFTS; 35°N, SAT), respective maximum throws are 2.9 (NFTS) and 1.9 km (SAT). The average throw along each fault is lower (~1.7 km, NFTS; ~1.0 km, SAT). The horizontal components of these thrust motions make up a considerable portion of the total shortening in the SBMs, which cumulatively represents 5% of the motion between the Pacific and North American Plates over the past few million years [*DeMets,* 1995].

The larger of the two thrust faults (NFTS) thus displays a significantly greater magnitude of slip. Interestingly, the difference in slip along each thrust fault seems to scale to fault length (70 km, NFTS; 50 km, SAT), in that both display maximum slip-to-length ratios of ~4×10^{-2}. This is a typical long-term value for large faults [*Cowie and Scholz,* 1992]. The greater magnitude of slip along the NFTS is consistent with the idea that it has played a more significant role in raising the Big Bear plateau. Given that the exact history of either fault remains uncertain, however, it is difficult to fully assess their relationship. The SAT may have been a secondary back thrust to the NFTS if coeval or simply a smaller, preexisting structure. The SAT has likely been inactive throughout much of the Quaternary [*Sadler,* 1993], but the NFTS also appears to have decelerated in the last few hundred thousand years. The maximum vertical displacement on the NFTS implies an average uplift rate of 0.83-0.55 mm/yr (net slip rate is 1.45-0.97 mm/yr) over the past 2-3 Myr [*May and Repenning,* 1982], whereas late Pleistocene scarps indicate slower rates of 0.05-0.30 mm/yr [*Meisling and Weldon,* 1989; *Bryant,* 1986]. Tighter constraint on fault timing is needed to test whether the opposing thrust faults acted independently or in concert to uplift the plateau and to determine whether the NFTS has slowed in the late Quaternary.

5.2. Architecture of Transpression-Related Structures in the SBMs

To synthesize our interpretations for the structural geometry of the SBMs, we have sketched a simple block diagram in Figure 13. The NFTS is shown as undercutting the SAT and nearly meets the San Andreas fault on the south. On the east the NFTS has a convex up shape, as it steepens to accommodate a greater component of vertical motion beneath Onyx Mountain. In the middle the NFTS is shown with a complex shape, flattening beneath the low Santa Ana Valley and steepening to explain the high San Gorgonio block. On the west the NFTS displays a more simple, listric shape. Although little data constrain the orientation of the SAT, its small size indicates that it is a minor backthrust to the NFTS. Together these thrust faults adequately account for the uplift of the Big Bear plateau, although whether they were coactive is not known. Imprinted across the entire plateau is a diffuse zone of dextral shear, whose mechanical role is not well understood. This system may postdate uplift, although existing fault history data and a lack of crosscutting relationships suggest the deformational systems may be coactive [*Spotila,* 1999].

It is significant that the NFTS can explain rock uplift in the San Gorgonio block. Minor high-angle faults add ~0.5 km of uplift to this block relative to Santa Ana Valley (Figure 9b), but no other structures are required. On the basis of thermochronometric isochron shapes [*Spotila et*

al., 1998], this block is a ~30-km-wide antiform that plunges gently northward. If the NFTS has uplifted this block, it must be confined to this narrow east-west extent. We have thus drawn a localized thrust patch that extends farther south than the eastern or western segments (Figure 13). This allows the NFTS to connect directly to the small convergent stepover at San Gorgonio Pass. It is in this vicinity that the greatest deformation has occurred, including the uplift of crustal slices along the high-angle strands of the San Andreas fault zone (Figures 7 and 9).

This synthesis bears similarities to two general conceptions of transpressive deformation. Given that the NFTS appears to undercut the SAT and extend southward to the San Andreas fault, a high-angle transpressive zone (i.e., flower structure [*Sylvester,* 1988; *Sadler*, 1982]) probably does not exist beneath the plateau. The core of the SBMs may thus be likened to a fold and thrust belt that internally deforms the crust adjoining a strike-slip fault zone (e.g., the western Transverse Ranges [*Namson and Davis,* 1988]). The more gently dipping sections of the NFTS may also be likened to a subhorizontal detachment [*Corbett,* 1984; *Li et al.*, 1992], which are predicted to decouple upper and lower crust along transpressive margins [*Beaudoin*, 1994; *Lemiski and Brown*, 1988]. However, our interpretation of NFTS shape is more complex. The eastern portion of the fault appears to steepen, rather than flatten, and the fault's complex shape is much more irregular than a uniformly shallow dipping decollement. Furthermore, the extreme rock uplift within the high-angle strands of the San Andreas fault zone on the south implies that a portion of the transpressive system does resemble the classic "flower structure" shape [*Spotila et al.*, 1998] (Figure 9b). Like the Spitsbergen transpressive orogen [*Lowell,* 1972] or other mountain systems with significant strike-slip motion [*Vauchez and Nicolas*, 1991; *Schwartz et al.*, 1990; *Lettis and Hanson*, 1991], the San Andreas fault zone appears to be a high-angle zone of partitioned lateral and vertical strain and is itself responsible for large magnitudes of rock uplift.

An added complication to the architecture of deformation is the presence of high-angle strike-slip faults within the upper plate of the NFTS (Figure 9). Faults of the eastern California shear zone that display significant dextral motion and have been active in the late Pleistocene are present both north of and within the plateau (Figure 2) [*Spotila,* 1999]. Because crosscutting relationships along fault traces have not been demonstrated, however, it is unknown how these relate to the NFTS [*Sadler,* 1982; *Miller,* 1987]. The trace of the NFTS bends southward where it meets the Helendale-Blackhawk faults, implying a possible right-lateral offset along the strike-slip system (Figure 2). The Helendale fault appears offset by the NFTS itself, however, as it steps right across a graben and connects to the Pipes Canyon fault within the plateau. Northward motion of the hanging wall block along the NFTS could have offset the trace of a once-continuous dextral fault between upper and lower plates. The mutually disrupted traces of the strike-slip and thrust faults could indicate that they have interacted synchronously during uplift. The possibility that these fault systems have been coactive illustrates an interesting dilemma of how intersecting fault systems of different kinematic behavior can work together to accommodate crustal deformation.

The structural array required to accommodate convergence in the SBMs is thus an intricate pattern of deformation that resembles several general notions of transpressive systems. Both high- and low-angle structures appear to have worked in concert to transform plate motion into orogeny. This three-dimensional pattern of faulting should improve models of seismogenic sources in the southern California region. Given that we now have a better idea of the geometry and kinematics of these structures, we can also address the mechanism responsible for transpression in the SBMs.

5.3. Source of Convergence in the SBMs

A distinct aspect of deformation in the SBMs is the narrowness of the region that has experienced significant horizontal shortening. The east to west distribution of convergence has a rough parabolic shape only a few tens of kilometers wide (Figure 7). This convergence is the only significant zone of transpressional deformation anywhere east of the San Andreas fault in southern California, and its peak intensity lies just northwest of a localized restraining bend in the transform fault. This spatial coincidence suggests a possible causal link between transpressional orogeny and strike-slip fault geometry.

Others have suggested that the San Gorgonio Pass left step has been responsible for convergent uplift of the SBMs [*Dibblee,* 1975; *Matti and Morton,* 1993; *Humphreys and Weldon,* 1994]. Our analysis now permits a quantitative comparison between convergent uplift and horizontal motion in the stepover. If the 15-km-wide left step is a true gap in right-lateral faulting, it should accumulate an excess volume of rock due to the 25 mm/yr fault-parallel motion on the northwest and southeast [*Weldon and Sieh,* 1985; *Sieh,* 1986]. If this geometry has been stable for the last 2 Myr, the excess volume of crust should have been ~11,250 km^3 (assuming a 15-km-thick brittle crust; Figure 14a). This value represents the maximum volume of rock that convergence in San Gorgonio Pass could have provided for crustal thickening in the lifetime of the SBMs. Our estimate of the volume of rock uplift in the SBMs is ~4400 km^3. If the anomalously deep seismicity below the SBMs represents depression of the brittle plastic transition due to forced rock subsidence, ~1300 km^3 of crustal thickening must be added to the rock uplift (based on seismicity of *Magistrale and Sanders* [1996] and assuming a 15-km-deep presubsidence brittle-plastic transition). This simple volume comparison implies that crustal thickening in the SBMs required addition of ~5700 km^3 of rock, or roughly half of what the left step in the San Andreas fault could have provided. The forceful addition of a large volume of rock in the stepover may thus have thus been responsible for the convergent rise and northward movement of the SBMs.

For the entire SBMs to have grown due to crustal thickening spawned by the San Gorgonio Pass stepover, however, their present-day spatial coincidence must have

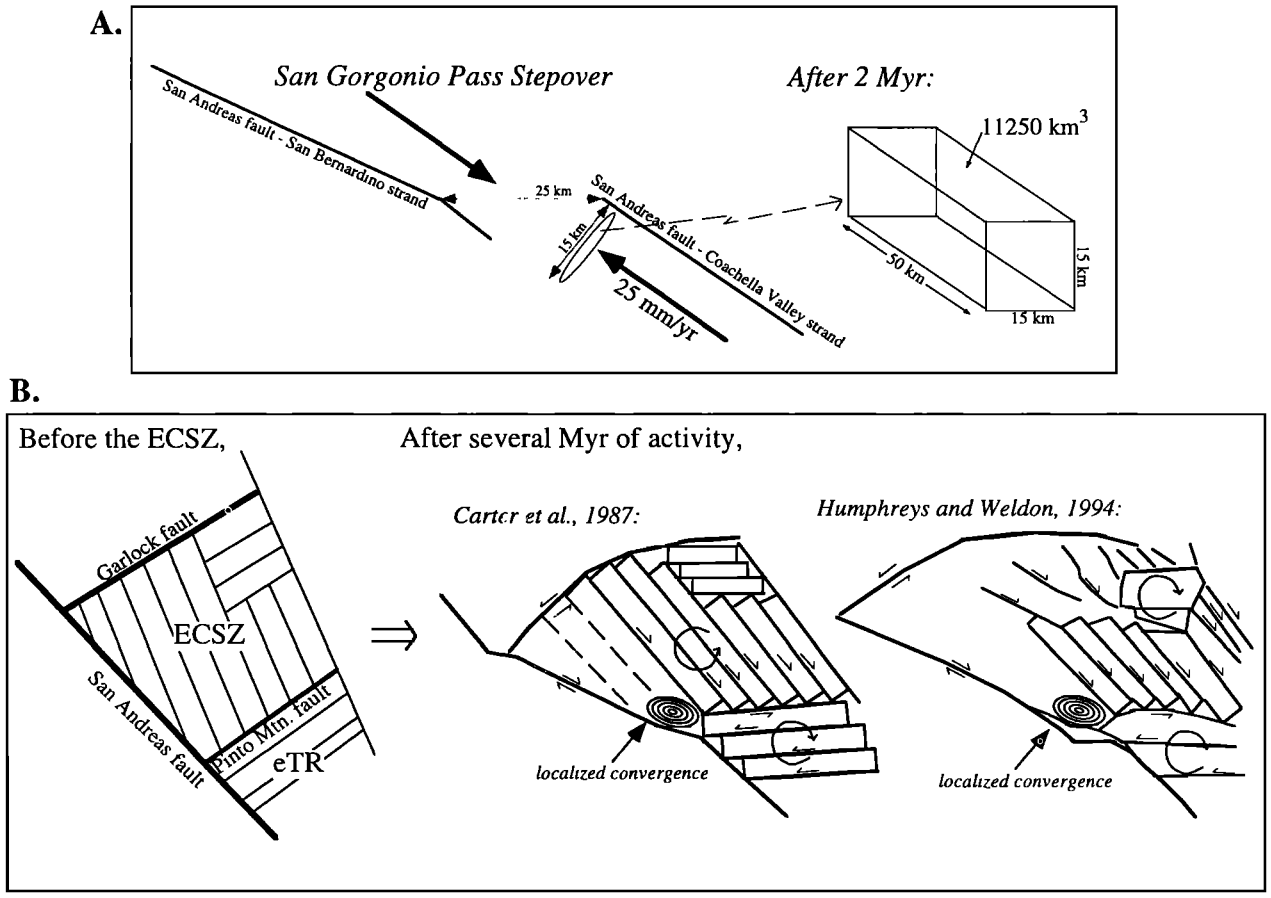

Figure 14. Plots illustrating that the SBMs may have been built in response to convergence at the restraining bend at San Gorgonio Pass. (a) Schematic diagram of the 15-km-wide left step in the San Andreas fault zone at San Gorgonio Pass. If there is zero lateral motion across this stepover, the 25 mm/yr rate along the San Andreas fault would create an excess crustal volume of 11,250 km^3 in 2 Myr. This is about twice as large as the volume of rock uplifted in the SBMs. (b) Two kinematic models of the San Andreas fault, eastern California shear zone, and easternmost Transverse Ranges showing that a left step should develop in the San Andreas fault at San Gorgonio Pass due to the transrotation of blocks to the east and left slip along the Pinto Mountain fault [after *Carter et al.*, 1987; *Humphreys and Weldon,* 1994]. Although magnitudes of slip and rotation to the east differ between the models, both imply that the left step in the San Andreas fault would be stationary relative to the deformational domains to the east, including the SBMs.

existed for the past several million years. This would have been possible only if the restraining bend has been fixed with respect to Mojave plate east of the San Andreas fault. If the stepover had instead been fixed with respect to the Peninsular Ranges, the thickened crust of the SBMs would have been steadily shuffled off toward the southeast. In this case, we would expect the SBMs to appear more like the steady-state topography of the Santa Cruz Mountains. This northern California range is highest and youngest at the small restraining bend in the San Andreas fault where it is forming but becomes older and decreases in elevation (due to erosion) in the direction of strike-slip motion [*Anderson,* 1990]. We must thus ask whether there are any geologic features to the east of the San Andreas fault that may have controlled the location of its left bend at San Gorgonio Pass.

The San Gorgonio Pass restraining bend presently lies at the junction of two distinct structural domains on the North American side of the San Andreas fault (Figure 1). To the northeast, the diffuse, northwest-trending eastern California shear zone has accumulated ~65 km of right-slip since the middle Miocene [*Dokka and Travis,* 1990]. This zone is a structural conduit for transferring slip from the San Andreas fault to the Basin and Range and presently accommodates ~12 mm/yr dextral shear [*Sauber et al.,* 1994]. To the southeast, the west-trending faults of the easternmost Transverse Ranges have accrued ~50 km of sinistral displacement in the past 10 Myr [*Powell,* 1981]. By rotating ~41° clockwise this system of left-lateral faults has accommodated 52-100 km of dextral shear, a value similar to the plate motion accommodated by the eastern California shear zone to the north [*Carter et al.,* 1987;

Dickinson, 1996]. At the boundary between the eastern California shear zone and easternmost Transverse Ranges lies the Pinto Mountain fault. This structure has a maximum of 17 km of left slip and connects directly to the San Andreas fault in the vicinity of San Gorgonio Pass [*Dibblee,* 1992]. The separation of the San Andreas fault in the stepover matches the magnitude and sense of motion along the Pinto Mountain fault, which implies that the restraining bend grew as crust to the east was displaced. *Matti and Morton* [1993] similarly proposed that the left bend grew while the Mission Creek fault was the active strand of the San Andreas fault zone, from roughly 3.5 to 0.5 Myr ago. The San Gorgonio Pass stepover may thus have remained fixed with respect to the North American side of the transform, consistent with the idea that the left bend was causally linked to the structural boundary between the transrotating domains to the northeast and southeast.

Two kinematic models of block rotation and strike-slip faulting in the eastern California shear zone and easternmost Transverse Ranges predict that a deflection in the San Andreas fault should have developed near San Gorgonio Pass over the last few million years. In one model [*Carter et al.,* 1987] clockwise rotation and left-lateral faulting to the southeast and slight counterclockwise rotation and dextral faulting in the Mojave create a slight left deflection in the San Andreas fault that is fixed to the boundary between the southern and northern transrotating domains (Figure 14b). A second model [*Humphreys and Weldon,* 1994], which uses a different interpretation of the rotation pattern to the northeast [cf. *Dickinson,* 1996], similarly results in a left deflection of the San Andreas fault at San Gorgonio Pass. Both of these kinematic models illustrate how the small left-bend in the San Andreas fault could have evolved at the western end of the boundary between two distinct structural domains to the northeast and southeast. In detail, the interaction of the San Andreas fault and these structural systems has likely been more complex and may have resulted in slight migration of the restraining bend with respect to North America [*Humphreys and Weldon,* 1994; *Johnson et al.,* 1994; *Dokka and Travis,* 1990]. To the first order, however, a mechanism of fixing the bend with respect to the SBMs seems to exist.

Because of their apparent long-term spatial coincidence, we propose that growth of the SBMs has been directly associated with the left-step in the San Andreas fault at San Gorgonio Pass. Our volume comparison implies that the crustal convergence in the stepover could have been more than twice that needed for crustal thickening in the SBMs. The excess convergence was likely avoided by lateral transfer of rock through the restraining bend (i.e., at half of the San Andreas fault's rate). If the SBMs have been built owing to convergence at San Gorgonio Pass, then their transpressive orogenesis has been the result of a local geometric complexity along a strike-slip fault. They may thus be distinct from the crustal thickening within the >200-km-wide western Transverse Ranges, which may be a more direct function of oblique plate motion [*Dickinson,* 1996; *Namson and Davis,* 1988]. However, the left step at San Gorgonio Pass may itself be the result of strike-slip and rotation within structural domains to the east. These domains accommodate plate motion and help the North America plate negotiate the Big Bend in the San Andreas fault (Figure 1), and thus the SBMs may ultimately be the product of obliquity between plate motion and the transform plate boundary. Alternative explanations for convergence in the SBMs, such as upper crustal convergence due to a negatively buoyant slab in the upper mantle [*Humphreys and Hager,* 1990], cannot be ruled out but seem unlikely given the symmetry of deformation about San Gorgonio Pass.

5.4. Implications for Seismic Hazards

The NFTS is a large structure with significant displacement, which has played a primary role in uplifting the SBMs over the past few million years. Because of its size and distance from the San Andreas fault it should be considered an independent structural component of the transpressive deformation system [*Lettis and Hanson,* 1991]. It thus represents a significant potential seismic hazard to the growing population of southern California's Inland Empire. Given that the 80-km-long thrust fault appears to have uplifted the entire Big Bear and San Gorgonio blocks, its down dip width is likely ~30 km (Figure 9). Its dimensions therefore imply a maximum-sized event of moment magnitude M_W = 7.5 (assuming ~3 m throw per event [*Wells and Coppersmith,* 1994] and rigidity equal to 3×10^{11} dyn/cm^2). This is as large as the major thrust events feared in metropolitan Los Angeles [*Dolan et al.,* 1995]. Such an event would also be quite damaging, based on the significant damage associated with the smaller (*M*6.5) Big Bear earthquake (1992). However, it is also possible that the NFTS fails only in small segments or is even inactive because of the degree to which it is intersected by northwest trending strands of the eastern California shear zone [*Sadler,* 1982]. These possibilities indicate the need for paleoseismic studies along the NFTS to quantify its future rupture capability.

6. Conclusions

The weathered surface atop the SBMs is a deformed structural datum that is useful for understanding the architecture and kinematics of transpressive uplift. On the basis of the vertical displacements measured along traces of the opposing thrusts of the Big Bear plateau the NFTS is the principle structure and the SAT is a minor backthrust within its hanging wall block. Together these thrusts have accommodated ~4 km of north-south horizontal convergence, a minor component of total Pacific-North America motion in the past few million years. On the basis of analysis of the shape of the overlying weathered surface the NFTS has a complex geometry at depth. The fault partly flattens into a decollement on the west, steepens to a convex up shape on the east, and is contorted beneath the central part of the range. Both the Big Bear plateau and San Gorgonio block appear to have risen along the NFTS, while oblique reverse motion along strands of the San Andreas fault zone is associated with uplift for crustal slivers to the south. The total horizontal plate

motion accommodated by uplift of these blocks is constrained by balancing the volume of rock uplift that is evident in the weathered surface and thermochronometry. Maximum convergence (6.3 km) occurs in the central part of the range just northwest of San Gorgonio Pass. Horizontal motion decreases rapidly to east and west, thus defining a very localized deformational pattern that is closely associated with the restraining bend in the San Andreas fault zone. This suggests that transpressive uplift of the SBMs has been produced by a localized geometric perturbation in the strike-slip system, which itself may have resulted from the transrotation of blocks within shear zones to the east.

Acknowledgments. We thank Egill Hauksson for help with seismicity data, Shawn Biehler for help modeling Bouguer gravity anomalies, Miles McKenney for sharing borehole data, and Doug Yule, Brian Wernicke, Ken Farley, Rob Clayton, Leon Silver, and Slawek Tulaczyk for ideas and comments throughout the course of this study. We also thank Peter Sadler and John Crowell for valuable reviews. This research was supported by the Southern California Earthquake Center (contribution 482), which is funded by NSF Cooperative Agreement EAR-8920136 and USGS Cooperative Agreements 14-08-0001-A0899 and 1434-HQ-97AG01718. Contribution 8593 of the Seismological Laboratory at the California Institute of Technology.

References

Allen, C R , San Andreas fault zone in San Gorgonio Pass, southern California, *Geol. Soc. Am Bull., 68*, 315-350, 1957.

Aksoy, R., P. Sadler, and S. Biehler, Gravity anomalies over sedimentary basins on the Helendale fault trend, in *Geology Around the Margins of the Eastern San Bernardino Mountains*, edited by M.A. Kooser and R.E Reynolds, pp. 121-128, Inland Geol. Soc., Redlands, Calif., 1986.

Anderson, R.S , Evolution of the northern Santa Cruz Mountains by advection of crust past a San Andreas fault bend, *Science, 249*, 397-401, 1990.

Beaudoin, B.C., Lower-crustal deformation during terrane dispersion along strike-slip faults, *Tectonophysics, 232*, 257-266, 1994.

Biehler, S., R.W. Tang, D.A. Ponce, and H.W. Oliver, Bouguer anomaly map of the San Bernardino Quadrangle, *Reg. Geophys. Map Ser., 3B*, Calif. Div. of Mines and Geol , 1988.

Brown, G., and Associates, Geology and groundwater geology of Big Bear Valley, in *Spring Field Trip*, pp. 73-95, *Assoc. of Eng. Geol., S. Calif. Sect.*, Los Angeles, Calif., 1976.

Bryant, W.A., Eastern North Frontal fault zone and related faults, southwestern San Bernardino County, *Fault Eval. Rep., FER 182*, Calif Div. of Mines and Geol., 1986.

Bull, W.B., Tectonic geomorphology of the Mojave Desert, *Contract Rep.*, 14-08-001-G-394, 188 pp , Off of Earthquakes, Volcanoes, and Eng., U S. Geol. Surv., Menlo Park, Calif , 1977.

Carter, J.N., B.P. Luyendyk, and R.R. Terres, Neogene clockwise rotation of the eastern Transverse Ranges, California, suggested by paleomagnetic vectors, *Geol Soc. Am Bull., 98*, 199-206, 1987.

Corbett, E J , Seismicity and crustal structure of southern California· Tectonic implications from improved earthquake locations, Ph.D. thesis, Calif. Inst. of Technol, Pasadena, 1984.

Cowie, P A., and C.H. Scholz, Displacement-length scaling relationships for faults· Data synthesis and discussion, *J. Struct. Geol., 14*, 1149-1156, 1992.

DeMets, C., Reappraisal of seafloor spreading lineations in the Gulf of California: Implications for the transfer of Baja California to the Pacific Plate and estimates of Pacific-North America motion, *Geophys. Res. Lett., 22*, 3545-3548, 1995.

Dewey, J F , R E Holdsworth, and R.A. Strachan, Transpression and transtension zones, in *Continental Transpressional and Transtensional Tectonics*, edited by R E. Holdsworth, R.A Strachan, and J F Dewey, *Geol. Soc. of London Spec. Publ., 135*, 1-14, 1998.

Dibblee, T.W., Geologic map of the San Gorgonio Mountain 15' Quadrangle, scale 1:62,500, *U.S. Geol. Surv. Misc Geol. Invest. Map, I-431*, 1964a.

Dibblee, T W., Geologic map of the Lucerne Valley 15' Quadrangle, scale 1:62,500, *U.S. Geol. Surv. Misc. Geol. Invest. Map, I-426*, 1964b

Dibblee, T.W., Geologic map of the Morongo Valley 15' Quadrangle, 1:62,500 scale, *U.S. Geol. Surv. Misc. Geologic Invest. Map*, I-517, 1967a.

Dibblee, T.W., Geologic map of the Old Woman Springs 15' Quadrangle, scale 1:62,500, *U.S Geol Surv. Misc. Geol. Invest Map, I-518*, 1967b.

Dibblee, T W., Geologic map of the Redlands 15' Quadrangle, scale 1.62,500, *U.S. Geol. Surv Open File Map, 74-1022*, 1974.

Dibblee, T W., Late Quaternary uplift of the San Bernardino Mountains on the San Andreas and related faults, in *San Andreas Fault in Southern California*, edited by J.C. Crowell, *Spec. Rep Calif. Div. of Mines and Geol., 118*, 127-135, 1975.

Dibblee, T.W , Geology and inferred tectonics of the Pinto Mountain fault, eastern Transverse Ranges, California, in *Deformation Associated With the Neogene Eastern California Shear Zone, Southwestern Arizona and Southeastern California, Spec. Publ. 92-1*, edited by S.M. Richard, pp. 28-31, San Bernardino Co. Museum Assoc., Redlands, Calif., 1992.

Dickinson, W R., Kinematics of transrotational tectonism in the California Transverse Ranges and its contribution to cumulative slip along the San Andreas transform fault system, *Spec. Pap Geol. Soc. Am , 305*, 46 pp , 1996.

Dokka, R K , and C.J Travis, Late Cenozoic strike-slip faulting in the Mojave Desert, California, *Tectonics, 9*, 311-340, 1990.

Dolan, J F., K. Sieh, T K. Rockwell, R.S Yeats, J. Shaw, J. Suppe, G.J. Huftile, and E.M. Gath, Prospects for larger or more frequent earthquakes in the Los Angeles metropolitan region, *Science, 267*, 199-205, 1995.

Feigl, K.L., A. Sergent, and D Jacq, Estimation of an earthquake focal mechanism from a satellite radar interferogram: Application to the December 4, 1992 Landers aftershock, *Geophys Res Lett., 22*, 1037-1040, 1995.

Hauksson, E.L., L M Jones, K. Hutton, and D Eberhart-Phillips, The 1992 Landers earthquake sequence. Seismological observations, *J Geophys. Res., 98*, 19,835-19,858, 1993

Humphreys, E D , and B H Hager, A kinematic model for the late Cenozoic development of southern CA crust and upper mantle, *J Geophys Res , 95*, 19,747-19,762, 1990

Humphreys, E.D , and R.J Weldon, Deformation across the western U.S. A local estimate of Pacific-North America transform deformation, *J. Geophys Res., 99*, 19,975-20,010, 1994.

Jacobs, S.E., Geology of a part of the upper Santa Ana River Valley, San Bernardino Mountains, San Bernardino County, California, M S. Thesis, 107 pp., Calif. State Univ., Los Angeles, 1982.

John S Murk Engineers, Inc., and LeRoy Crandall and Associates, Historic and present conditions, upper Mojave River basin, Mojave Water Agency, Apple Valley, Calif , 1985

Johnson, H.O , D C Agnew, and F.K Wyatt, Present-day crustal deformation in southern California, *J. Geophys Res., 99*, 23,951-23,974, 1994

Jones, L E , and S E Hough, Analysis of broadband records from the June 28, 1992 Big Bear earthquake Evidence of a multiple-event source, *Bull. Seismol. Soc. Am., 85*, 688-704, 1995

Jones, L M , L K Hutton, D D. Given, and C.R Allen, The North Palm Springs, California, earthquake sequence of July, 1986, *Bull. Seismol. Soc. Am , 76*, 1830-1837, 1986.

King, G.C., R.S. Stein, and J.B. Rundle, The growth of geological structures by repeated earthquakes, 1, Conceptual framework, *J. Geophys. Res., 93*, 13,307-13,318, 1988

Lemiski, P J., and L D. Brown, Variable crustal structure of strike-slip fault zones as observed on deep seismic reflection profiles, *Geol Soc. Am. Bull., 100*, 665-676, 1988

Lettis, W R., and K.L Hanson, Crustal strain partitioning: Implications for seismic-hazard assessment in western California, *Geology, 19*, 559-562, 1991

Li, Y.-G., T.L. Henyey, and P.C. Leary, Seismic reflection constraints on the structure of the crust beneath the San Bernardino Mountains, Transverse Ranges, southern California, *J Geophys. Res., 97*, 8817-8830, 1992.

Lowell, J D , Spitsbergen Tertiary orogenic belt and the Spitsbergen fracture zone, *Geol. Soc Am. Bull., 83*, 3091-3102, 1972.

Magistrale, H , and C Sanders, Evidence from precise earthquake hypocenters for segmentation of the San Andreas fault in San Gorgonio Pass, *J Geophys Res , 101*, 3031-3044. 1996.

Matti, J.C , and D M. Morton, Paleogeographic evolution of the San Andreas fault in southern California: A reconstruction based on a new cross-fault correlation, in *The San Andreas Fault System. Displacement, Palinspastic Reconstruction and Geologic Evolution*, edited by R.E. Powell, R.J. Weldon, and J.C. Matti, *Mem. Geol. Soc. Am., 178*, 107-160, 1993.

May, S.R , and C.A Repenning, New evidence for the age of the Old Woman sandstone, Mojave Desert, California, in *Geologic Excursions in the Transverse Ranges*, edited by J.D. Cooper, pp. 93-96, *Geol. Soc Am. Cordilleran Sect. Meet. Guidebook, 78*, 1982.

Meigs, A , N Brozovic, and M.L. Johnson, Steady, balanced rates of uplift and erosion of the Santa Monica Mountains, California, *Basin Res., 11*, 59-73, 1999.

Meisling, K.E., Neotectonics of the north frontal fault system of the San Bernardino Mountains: Cajon Pass to Lucerne Valley, California, Ph D thesis, 394 pp., Calif. Inst. Technol., Pasadena, 1984.

Meisling, K E , and R J Weldon, Late Cenozoic tectonics of the northwestern San Bernardino Mountains, southern California, *Geol. Soc. Am. Bull., 101*, 106-128, 1989.

Miller, F.K., Reverse-fault system bounding the north side of the San Bernardino Mountains, in *Recent Reverse Faulting in the Transverse Ranges, California, U.S. Geol. Surv. Prof Pap., 1339*, 83-95, 1987.

Mount, V.S., and J. Suppe, State of stress near the San Andreas fault: Implications for wrench tectonics, *Geology, 15*, 1143-1146, 1987.

Namson, J , and T. Davis, Structural transect of the western Transverse Ranges, California: Implications for lithospheric kinematics and seismic risk evaluation, *Geology, 16*, 675-679, 1988.

Neville, S L., Late Miocene alkaline volcanism, south-central Mojave Desert and northeast San Bernardino Mountains, California, M.S Thesis, 143 pp., Univ. of Calif , Riverside, 1983.

Oberlander, T M , Morphogenesis of granitic boulder slopes in the Mojave Desert, California, *J Geol., 80*, 1-20, 1972.

Ollier, C D , *Weathering*, 304 pp., Addison-Wesley-Longman, Reading, Mass., 1975

Powell, R.E., Geology of the crystalline basement complex, eastern Transverse Ranges, southern California, Ph.D. thesis, Calif. Inst. of Technol., Pasadena, 1981.

Riley, F.S., Data on water wells in Lucerne, Johnson, Fry, and Means Valleys, San Bernardino County, California, *Open File Rep.*, 149 pp., U.S. Geol. Surv. and Calif. Div. of Water Resources, Long Beach, Calif., 1956.

Rzonca, G.F , and D.W. Clark, Local Geology, Kaiser Cement Corporation, Cushenbury Facility, Lucerne Valley, California, in *Geology and Mineral Wealth of the California Transverse Ranges*, edited by D.L. Fife and J.A Minch, pp. 676-679, S. Coast Geol Soc., Santa Ana, Calif., 1982

Sadler, P M , Provenance and structure of late Cenozoic sediments in the northeast San Bernardino Mountains, in *Geologic Excursions in the Transverse Ranges*, edited by J.D. Cooper, pp. 83-91, *Geol. Soc. Am Cordilleran Sect. Meet. Guidebook, 78*, 1982.

Sadler, P.M , The Santa Ana basin of the central San Bernardino Mountains: Evidence of the timing and uplift and strike-slip relative to the San Gabriel Mountains, in *The San Andreas Fault System: Displacement, Palinspastic Reconstruction, and Geologic Evolution*, edited by R.E Powell, R.J. Weldon, and J C. Matti, *Mem. Geol. Soc. Am., 178*, 307-322, 1993.

Sadler, P.M., and W.A. Reeder, Upper Cenozoic, quartzite-bearing gravels of the San Bernardino Mountains, southern California; recycling and mixing as a result of transpressional uplift, in *Tectonics and Sedimentation Along Faults of the San Andreas System*, edited by D.W Anderson and M.J Rymer, pp. 45-57, Soc. Econ. Paleontol. and Mineral., Pacific Sect., Los Angeles, Calif., 1983.

Sauber, J., W. Thatcher, S C Solomon, and M. Lisowski, Geodetic slip rate for the eastern California shear zone and the recurrence time of Mojave desert earthquakes, *Nature, 367*, 264-266, 1994.

Savage, J.C., and L.M. Hastie, Surface deformation associated with dip-slip faulting, *J. Geophys. Res., 71*, 4897-4904, 1966.

Schwartz, S.Y., D.L. Orange, and R.S. Anderson, Complex fault interactions in a restraining bend on the San Andreas fault, southern Santa Cruz Mountains, California, *Geophys. Res. Lett., 17*, 1207-1210, 1990.

Sieh, K.E., Slip rate across the San Andreas fault and prehistoric earthquakes at Indio, California (abstract), *Eos Trans AGU, 67 (44)*, 1200, 1986.

Spotila, J.A., The neotectonics of the San Bernardino Mountains and adjacent San Andreas fault. A case study of uplift associated with strike-slip fault systems, Ph D thesis, 378 pp., Calif Inst. of Technol., Pasadena, 1999.

Spotila, J.A., K.A. Farley, and K Sieh, Uplift and erosion of the San Bernardino Mountains associated with transpression along the San Andreas fault, California, as constrained by radiogenic helium thermochronometry, *Tectonics, 17*, 360-378, 1998.

Sylvester, A G , Strike-slip faults, *Geol. Soc Am. Bull., 100*, 1666-1703, 1988.

Teyssier, C , B. Tikoff, and M Markley, Oblique plate motion and continental tectonics, *Geology, 23*, 447-450, 1995.

Twidale, C.R , The origin and implications of some erosional landforms, *J Geol , 98*, 343-364, 1990

Vauchez, A , and A Nicolas, Mountain building· Strike-parallel motion and mantle anisotropy, *Tectonophysics, 185*, 183-201, 1991.

Webb, T H., and H. Kanamori, Earthquake focal mechanisms in the eastern Transverse Ranges and San Emigdio Mountains, southern California, and evidence for a regional decollement, *Bull. Seismol. Soc. Am., 75*, 735-757, 1985.

Weldon, R.J., and K.E. Sieh, Holocene rate of slip and tentative recurrence interval for large earthquakes on the San Andreas fault in Cajon Pass, southern California, *Geol Soc Am. Bull., 96*, 793-812, 1985.

Wells, D L , and K J. Coppersmith, New empirical relationships among magnitude, rupture length, rupture width, rupture area, and surface displacement, *Bull. Seismol Soc. Am , 84*, 974-1002, 1994.

Wilcox, R.E , T.P. Harding, and D.R. Seely, Basic wrench tectonics, *Am. Assoc. Petrol. Geol Bull., 57*, 74-96, 1973.

Willingham, C R , Gravity anomaly patterns and fault interpretations in the San Bernardino Valley and western San Gorgonio Pass area, southern California, in *Geology of the San Jacinto Mountains*, pp. 164-174, S. Coast Geol. Soc., Santa Ana, Calif., 1981.

Woodburne, M.O., Cenozoic stratigraphy of the Transverse Ranges and adjacent areas, southern California, *Spec. Pap. Geol. Soc. Am., 162*, 91 pp., 1975.

Woodford, A O., and T.F. Harriss, Geology of Blackhawk Canyon, San Bernardino Mountains, California, *Univ. Calif. Publ. Geol. Sci , 17*, 265-304, 1928

K Sieh, Division of Geological and Planetary Sciences, 100-23, California Institute of Technology, Pasadena, CA 91125

J Spotila, Department of Geological Sciences, Virginia Polytechnic Institute and State University, 4044 Derring Hall, Blacksburg, VA 24061 (spotila@vt edu)

(Received July 2, 1999,
revised January 7, 2000;
accepted April 7, 2000)